California Institute of Technology
Division of Geological and Planetary Sciences
Seismological Laboratory
Pasadena, California 01109

See 1473

Final Report

1 June 1972 - 30 November 1975

ARPA Order No:	2134
Program Code:	2F10
Contractor:	California Institute of Technology
Effective Date of Contract:	1 June 1972
Contract Expiration Date:	30 November 1975
Amount of Contract:	$273,078
Contract Number:	F44620-72-C-0083, P00001
Principal Investigators:	Charles B. Archambeau (1972 - 73) Donald V. Helmberger (213) 795-6811
Program Managers:	Lt. Col. Donald W. Klick (202) 694-5275 Mr. Bill Best (202) 693-0162
Title:	Near Field Small Earthquake Long Period Array

Sponsored by
Advanced Research Projects Agency
ARPA Order No. 2134

TABLE OF CONTENTS

SUMMARY

This final report describes the accomplishments achieved during the last year of our efforts towards a better understanding of the seismic radiation from earthquakes. Applying the techniques discussed in earlier reports on calculating the synthetic response generated by shear dislocation sources in a layered media we have endeavored to separate source effects from those due to propagation in the earth. The main objective here is an accurate scaling law of duration versus moment to be used in discrimination studies. The observations used in this report are of two types, those that are large enough to be studied teleseismically where one must separate the phases P, pP and sP etc, and those that are too small to be observed at large distances and must be studied locally. Thus our efforts have been divided into two sections, to model local broadband observations of moderate size earthquakes, and secondly, to apply our recently developed generalized inversion theory to the problem of obtaining source determinations based on teleseismic long and short period body waves.

In collaboration with Lane Johnson we investigated some of his broadband observations of central California earthquakes as recorded on opposite sides of the San Andreas fault zone. The earthquake mechanisms were of the strike-slip type occurring along the fault at epicentral distances less than 30 km. The seismograms obtained at the two sites are distinctly dissimilar in waveshape and amplitude even though they are at roughly the same azimuth. We found that these effects can be explained by a two layer upper-crustal model appropriate for

each site.

The results determined by matching the observations synthetically indicate that the durations for these events with M_L = 3.5 to 5 are about .3 to .6 seconds respectively and that accurate estimates of such parameters can only be accomplished after a detailed appreciation of receiver structure.

For the large events, magnitudes greater than 6, we adapted a generalized linear inverse technique for determining the source parameters from body wave data at teleseismic ranges, Δ = 30 to 90 degrees. The technique has been applied successfully to several events but we will restrict ourselves in this report to Borrego Mountain earthquake of April 9, 1968. Synthetic seismograms computed from the resulting model match in close detail the first 25 seconds of long period seismograms from a wide range of azimuths. The main shock source time function has been determined by a new simultaneous short period-long period deconvolution technique as well as by the inversion technique. The duration and shape of this time function indicate that most of the body wave energy was radiated from a surface with effective radius of only 8 km. This is much smaller than the total surface rupture length of the length of the aftershock zone. Along with the moment determination of $M_o = 11.2 \times 10^{25}$ dyne-cm, this radius implies a high stress drop of about 96 bars.

A plot of stress drop versus duration for events determined by fitting waveforms in the time-domain suggests that larger events may have higher stress drops than smaller events at least for the California

examined in this report.

I. INTRODUCTION

The main purpose of the "Joint Experiments on the spectra of Earthquake Source" was to determine the detailed nature of the seismic radiation from small earthquakes. Although the fundamental objective was to investigate discrimination criteria, this study was also aimed at understanding the basic physics involved in terms of detailed seismic sources as opposed to propagational effects.

Our work under this contract has been divided into three major tasks: (1) Field operations in Bear Valley, (2) Investigations of wave propagation theory for the modeling of earthquakes, (3) Data analysis and interpretation of existing data.

Unfortunately, the Bear Valley operation did not produce a particularly good data set due to lack of seismic activity. Furthermore, it was discovered in a study described in a previous report that a detailed appreciation of the receiver structure must be accomplished before one can determine accurate estimates of source parameters. This means that the best way to obtain accurate source parameters is to study many observations at the same station since the effects due to structure just below the station are common to all of the observations thus allowing recognition of features common to the site as opposed to source characteristics. For this reason much of our efforts have gone into a careful investigation of the excellent data set obtained from the San Andreas Geophysical Observatory working in cooperation with Lane Johnson. We will also report on some work done by graduate students, Larry Burdick, George Mellman and Tom Heaton on the Borrego

Mountain earthquake with attempts at explaining details of both the teleseismic and local observations.

The second task, (2) on the investigation of wave propagation theory for the modeling of earthquakes, has been discussed at length in earlier reports and can be found in the journals, see Helmberger (1974), Langston and Helmberger (1975) and Helmberger and Malone (1975).

We should also mention that a large amount of aftershock data was collected at the Oroville site. However, we exhausted our Air Force resources in the data collection and are unable to present the results at this time. We are hopeful that another agency will support the data analysis required and we will report on these results at a later date.

II. SOURCE PARAMETERS OF MODERATE SIZE EARTHQUAKES

Recent demands for scaling laws for various size earthquakes has greatly increased interest in local observations of

moderate size events in the range M_L = 4. to 5.5. That is, events that are too small to be well recorded teleseismically but large enough not to be commonly included in aftershock sequences. Most attempts at extracting the source parameters from such local observations have used the corner frequency approach where one makes no effort to separate source generated effects from propagational effects introduced by local crustal structure but works with the spectral characteristics of the entire record, see example Thatcher and Hanks (1973). While this study has been significant in establishing the importance of duration or corner frequency in relation to the other source parameters, it has not resolved the meaning of the large scatter in stress drops. For instance does a low stress drop event, long duration with a small moment, correspond to analyzsing a surface wave as a body wave?

Observations nearly above the event helps to minimize these propagation distortions but separating near-field from far-field effects for an event that is not well located is extremely difficult.and secondly, it is not often that a moderate size event occurs directly under a broad-band instrument capable of remaining in operation.

Some of the best observations at short distances have been recorded at the San Andreas Geophysical Observatory (SAGO) in central California and will be examined in this study where we will attempt to separate source effects from distortions caused by crustal structure.

The locations of the events relative to the two broadband stations SAGO-Central and SAGO-East, are given in Figure 1. SAGO-E is situated near exposed pliocene sedimentary rocks with outcrops of Franciscan to the northeast whereas SAGO-C is setting on granitic rocks of the Gabilan range. The earthquakes farther to the south are of the right-lateral transcurrent type

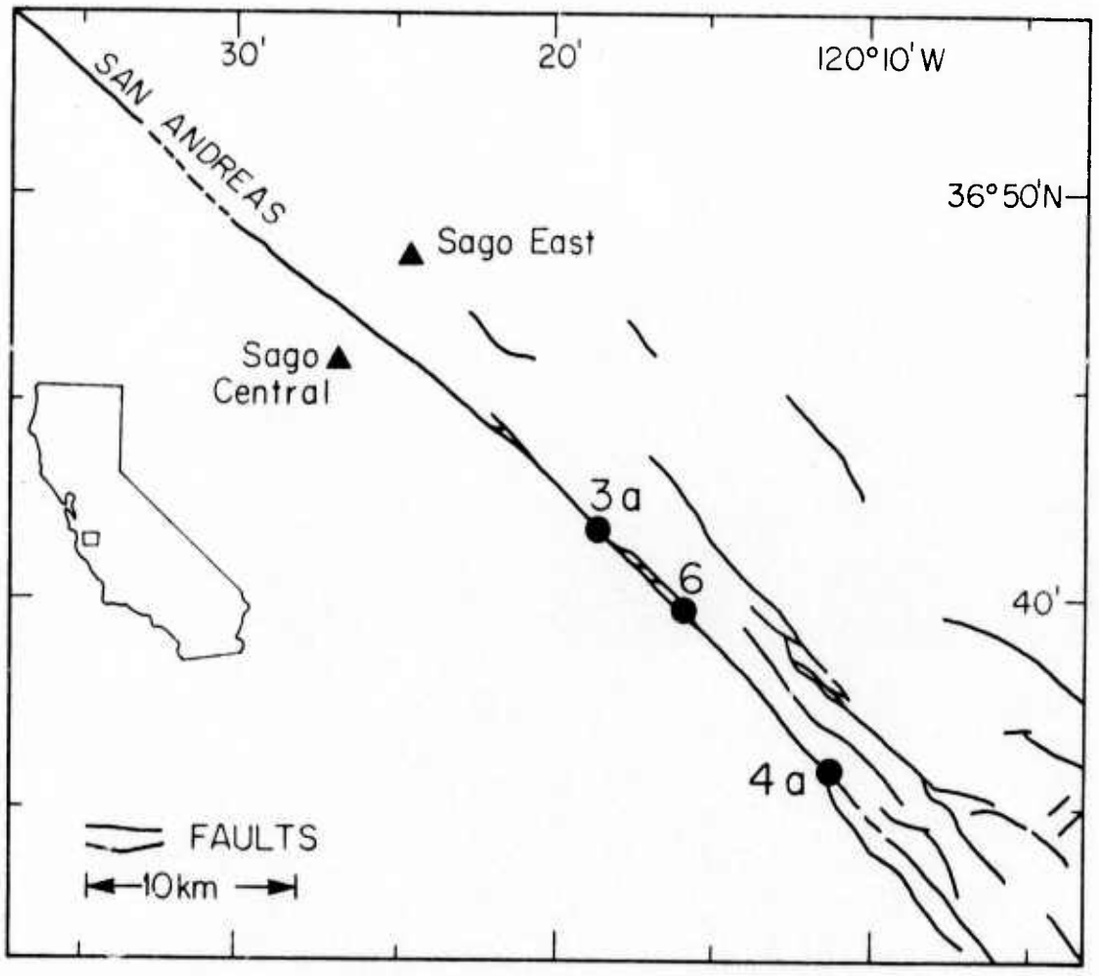

Figure 1. A map of a section of the San Andreas fault in Central California showing the locations of the seismographic stations SAGO-Central and SAGO-East relative to the three earthquakes studied. The identification numbers key the earthquakes to Table 1.

with focal mechanism parameters given in Table 1, after Johnson and McEvilly (1975). The observations are displayed in Figure 2 where it is clear that the similarity of the various events at each station is far greater than the similarity of the same event at each station. Note that the amplitudes are about a factor of two to three greater at SAGO-E as well. The three observations at SAGO-E are not only similar to each other they also look much like the waveforms observed along a profile running parallel to the fault discussed by Helmberger and Malone (1975). Example observations are given in Figure 3 along with synthetics generated for a simple one layer over a halfspace model. The first peak corresponds to the direct generalized ray, the second peak to the first multiple reflection, etc. These reflections occur near the receiver and move back towards the source as the number of reflections increase, for example the first multiple reflects off the surface at about 1.5 km from the receiver, the second reflection at 3 km, etc. Comparing the synthetic with the observation indicates that the fit is relatively good for about the first 10 sec which are described by the first 4 or 5 rays, and thereafter the fit rapidly deteriorates. We interpret this phenomenon as due to an imperfect surface waveguide that does not support the high degree of coherency necessary for the complete Love wave development but is locally well behaved. It thus appears that much of the complexity observed on local seismograms and their corresponding spectra can be explained in terms of upper crustal structure near the seismographic station. We investigate this hypothesis further in this paper where we will attempt to model the observations of Figure 2 synthetically.

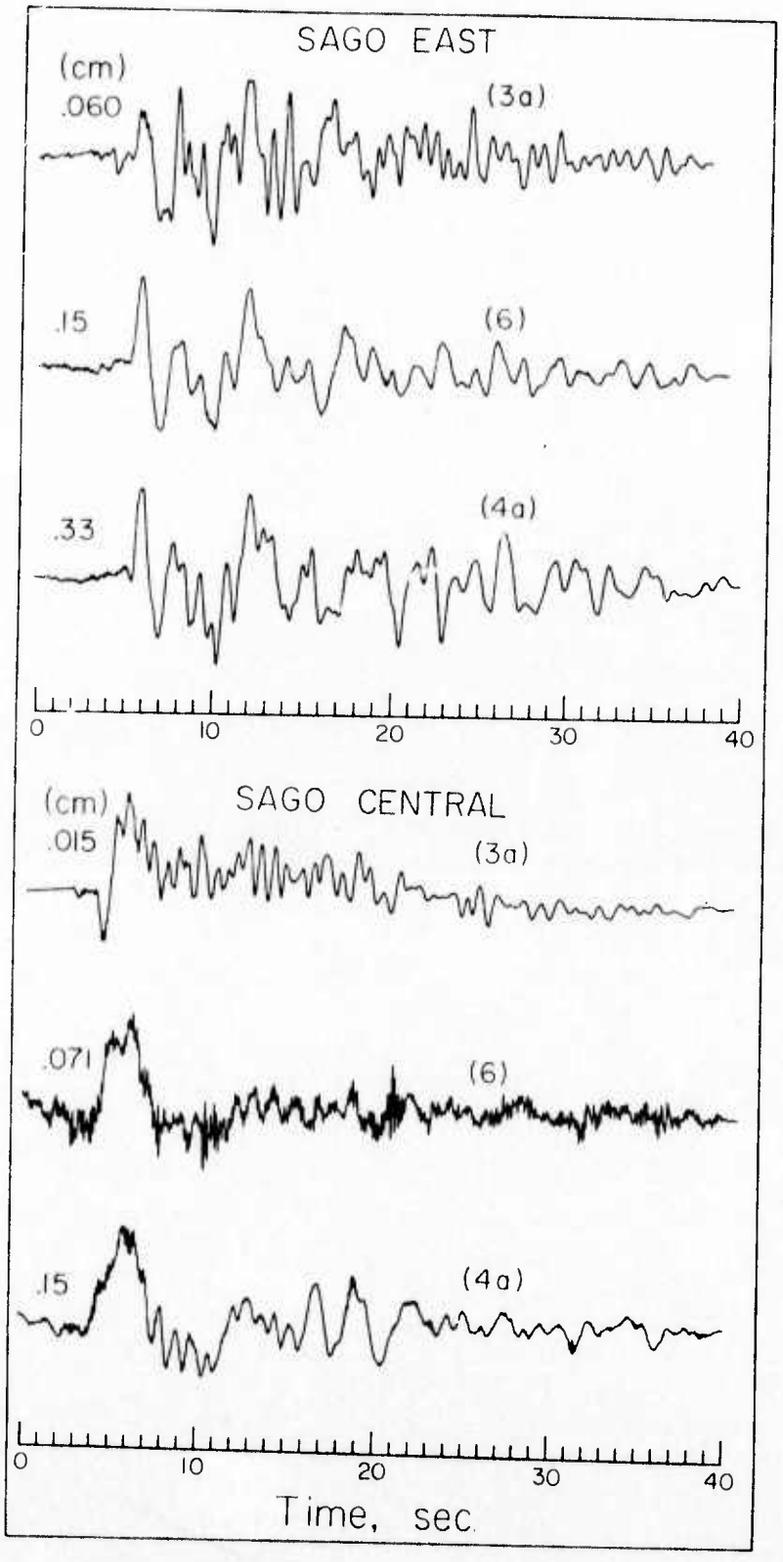

Figure 2. The tangential displacement seismograms (SH-components) at SAGO-East (top) and SAGO-Central (bottom) for events (3a), (6), and (4a). The original NS and EW seismograms are displayed in Figures 19 and 20 of Johnson and McEvilly (1974).

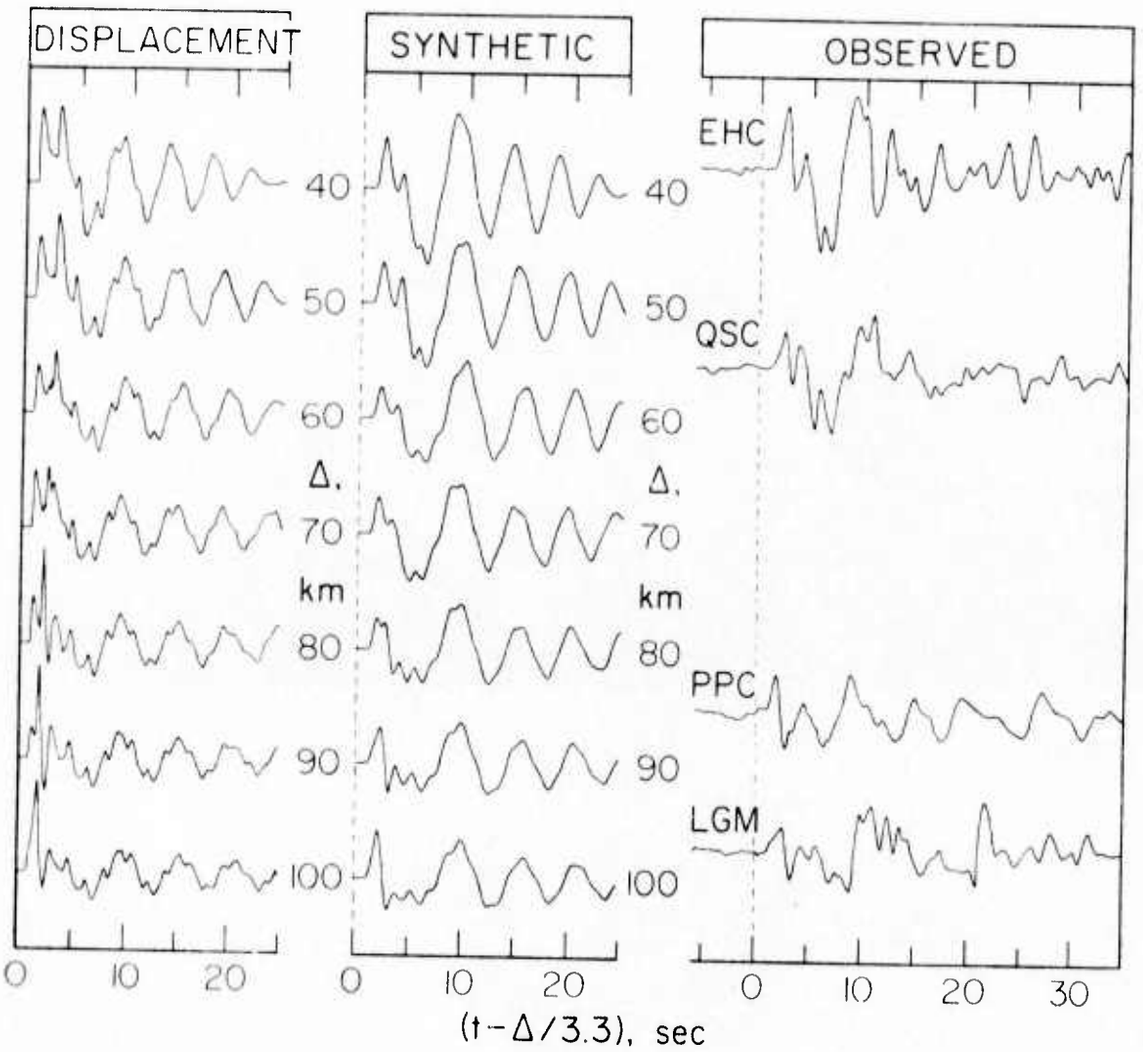

Figure 3. Comparison of synthetics with observations with all traces plotted on the same amplitude scale. The moment is determined by overlay to be 2.1 x 10^{22} ergs.

ANALYSIS

The strategy used in the model determination was simply to match the first ten seconds of observations for one of the events with the fewest number of parameters (layers) and to predict the behaviors at the other two ranges. We assume that these strike-slip earthquakes can be replaced by a point shear dislocation and the motion is controlled by pure SH type motion at these azimuths. The matching procedure is basically a trial and error technique where a starting model is assumed. Next, the corresponding displacement for an assumed source excitation is constructed along with the synthetic seismogram. After comparing the synthetic with the observation in question and previous attempts one makes the appropriate alterations in the model and repeats the process. Since we know more about the structure on the east from the previous study, we initiate the above procedure on SAGO-E at Δ = 30 km.

MODELING SAGO-E

As a starting model we used model A proposed by Helmberger and Malone (1975) derived from observations obtained approximately 30 km to the east of the fault. Using the appropriate SAGO-E instrument resonse as described by Johnson and McEvilly (1975) one obtains the synthetics in Figure 4. We assumed a far-field source time function, F(5), of trapezoidal form described by δt_1, δt_2 and δt_3 as shown schematically in the right-hand corner of Figure 4a. The comparison with the observed record is made in overlay format. A reduction in the size of the first peak relative to later arrivals can be achieved by simply reducing the source depth but the overswing or the size of the first trough can not be obtained so easily. Of course, this feature can be obtained by allowing the fault to overshoot producing a time function as shown in the right-hand corner of Figure 4b.

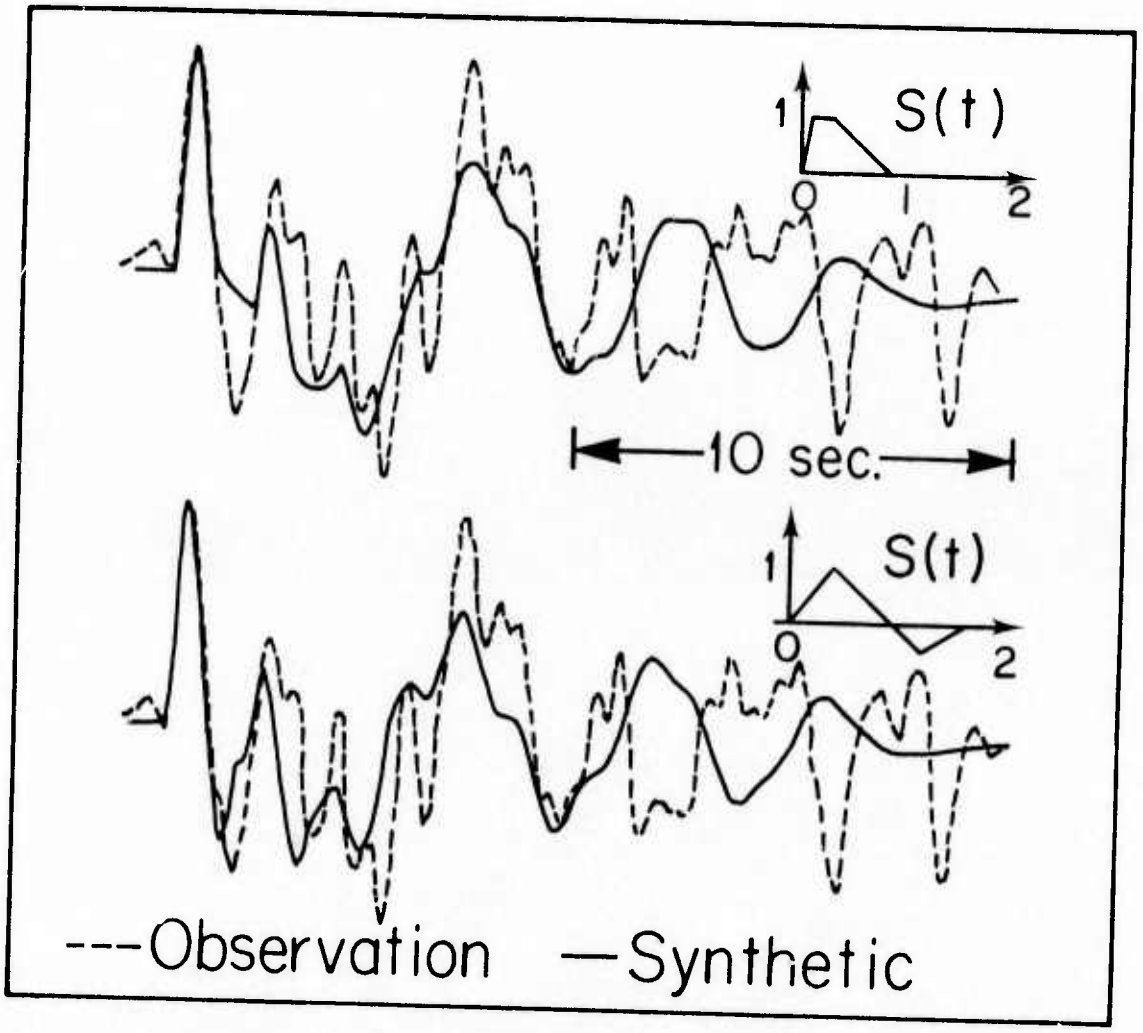

Figure 4. Comparison of synthetics generated from the model A of Helmberger and Malone (1975) with SAGO-E for the (4a) event.

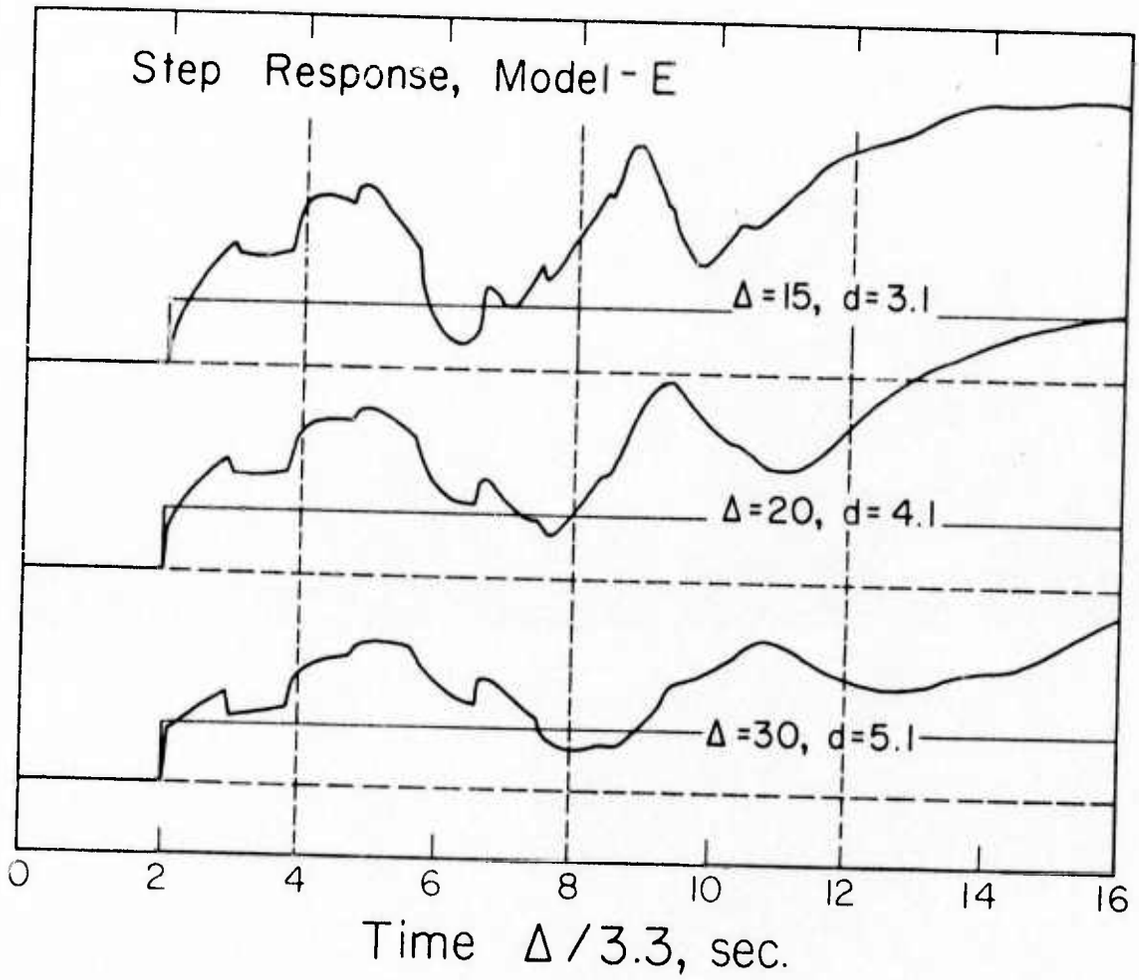

Figure 5. Step function responses as a function of range, Δ, and depth, d, for model E. The first-motion approximation to the far-field response (optics) appropriate for a halfspace is included for comparison.

This feature produces a possible solution but a simpler explanation is obtained by introducing a layer of low velocity material (sediments) at the surface. These sediments are exposed along the eastern edge of the fault and are apparent as travel time dealsy (Boore and Hill, 1973). With the addition of this low velocity layer we have essentially four parameters to vary. After a diligent search we obtained model-E given in Table 2 with corresponding step responses given in Figure 5. These results are similar to those presented in Helmberger and Malone (1975) at the longer periods but they have a strong one second periodicity produced by the soft superficial layer. The comparison of the corresponding synthetics with the SAGO-E observations is displayed in Figure 6. To reduce the number of parameters we assumed $\delta t_1 = \delta t_2 = \delta t_3 \equiv \delta t$ and picked the best fitting δt allowing δt to vary from .1 to 1. The moment is determined by scaling the synthetic to the corresponding observation. The rsults are given in Table 3. Note that we adjusted the depths somewhat essentially making all three events shallower. These changes are well within epicentral depth locations as determined from travel times and was done to produce the relative strengths of the first arrival to later arrivals. Changing the epicentral depth is quite effective for this purpose as discussed by Helmberger and Malone (1975).

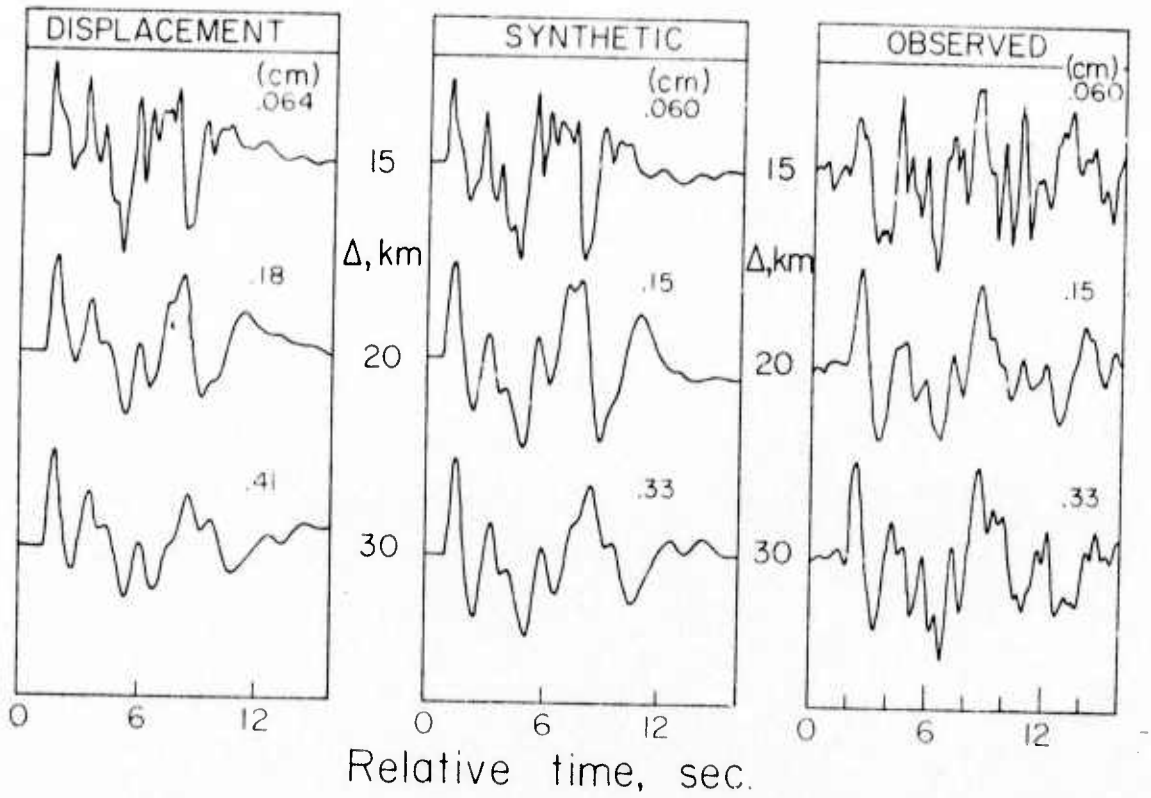

Figure 6. Comparison of synthetics with observations at SAGO-E with the amplitudes given in cm. The source parameters used are given in Table 3.

MODELING SAGO-C

For the western model, we draw from two studies one by Mellman and Helmberger (1974) on diffraction effects caused by a high velocity layer, the other by Boore and Hill (1973) who obtained a shear velocity of about 3.5 km/sec for the gravitic rocks. We thus assumed a layer (β = 3.5 km/sec) over a halfspace (β = 2.5 km/sec) as a preliminary model to test for the effects diagnositc of a lower velocity zone at depth. The results are displayed in Figure 7 where the responses are at the same range with the layer thickness as the only variable.

Most of the short period energy is reflected into the halfspace when the layer is thin; that is the transmission coefficient for the direct ray (onset time) changes by over a factor of three going from h = 1 to 4 km. There is also considerable interference of the multiple reflections as is evident from the gilchs near the beginning. In general, the polarity of these multiples will oscillate since the reflection coefficient is positive at the base of the layer. The large increase in amplitude a few seconds after the onset is essentially the direct arrival as h goes to zero. This effect is produced by the shape of the Cagniard contour as discussed by Helmberger and Malone (1975) and Mellman and Helmberger (1974).

Applying the experience learned from this example, we attempted to find a model that would produce the proper broadening of the first pulse that is so evident in Figure 2. After investigating many two layer models of various combinations of velocities we obtained model W given in Table 2 with the step responses and corresponding synthetics given in Figures 8 and 9. The amplitudes of the synthetics are appropriate for the moments as deduced from the SAGO-E observation

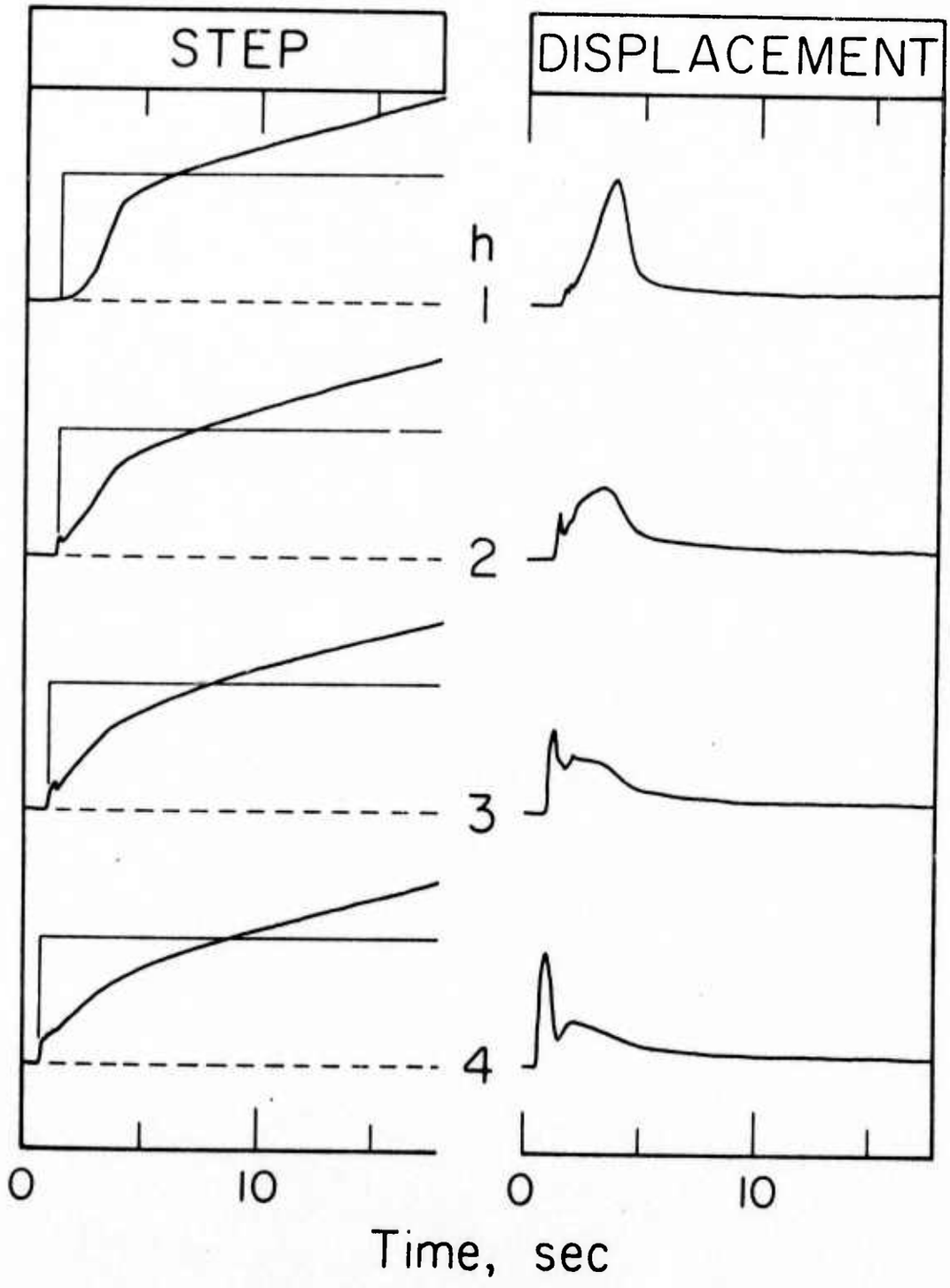

Figure 7. Step and displacement responses for various layer thicknesses at a range of 30 km with the strike-slip source at a depth of 6 km. The source duration parameters are δt_1 = .1, δt_2 = .2 and δt_3 = .5 seconds.

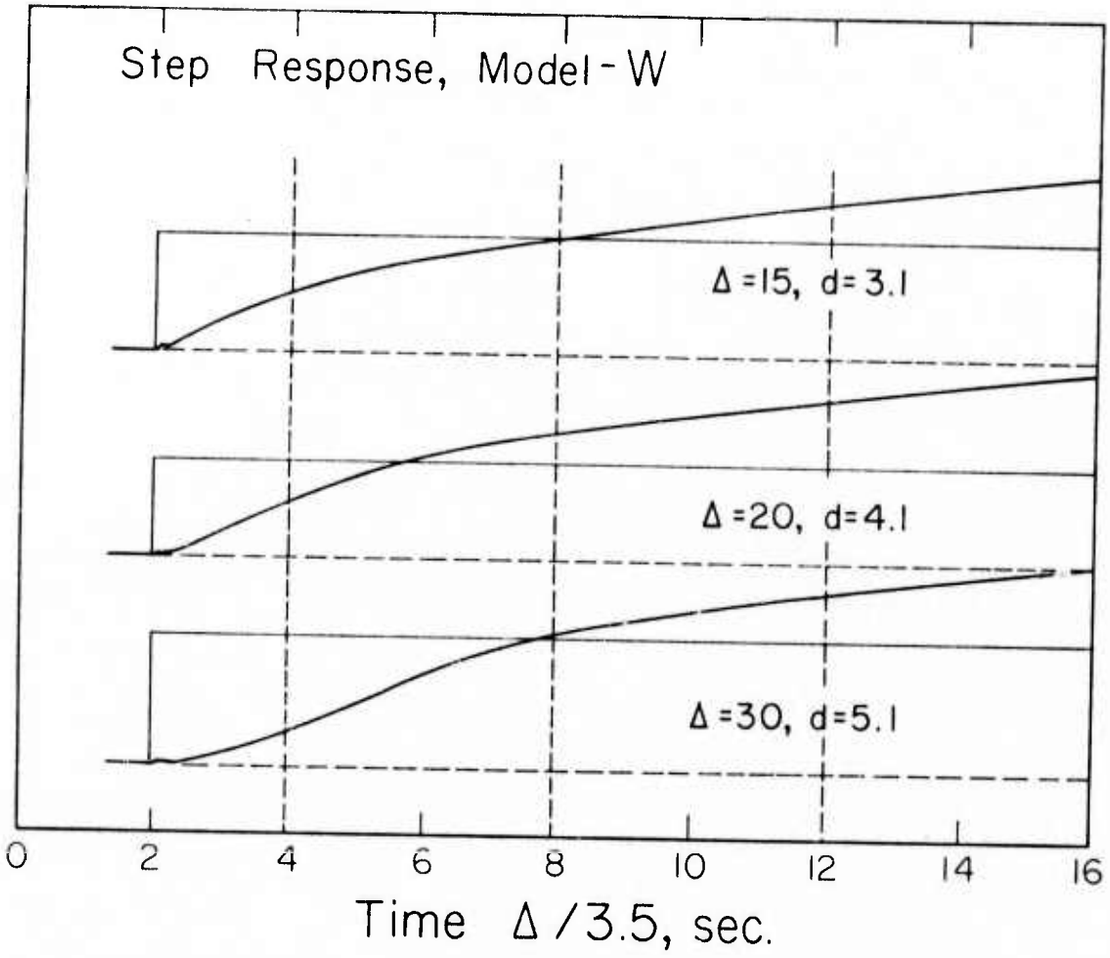

Figure 8. Step function responses as a function and range and depth for model W. The first-motion approximation of the far-field response for a halfspace with a model parameters appropriate for the bottom material is included for comparison.

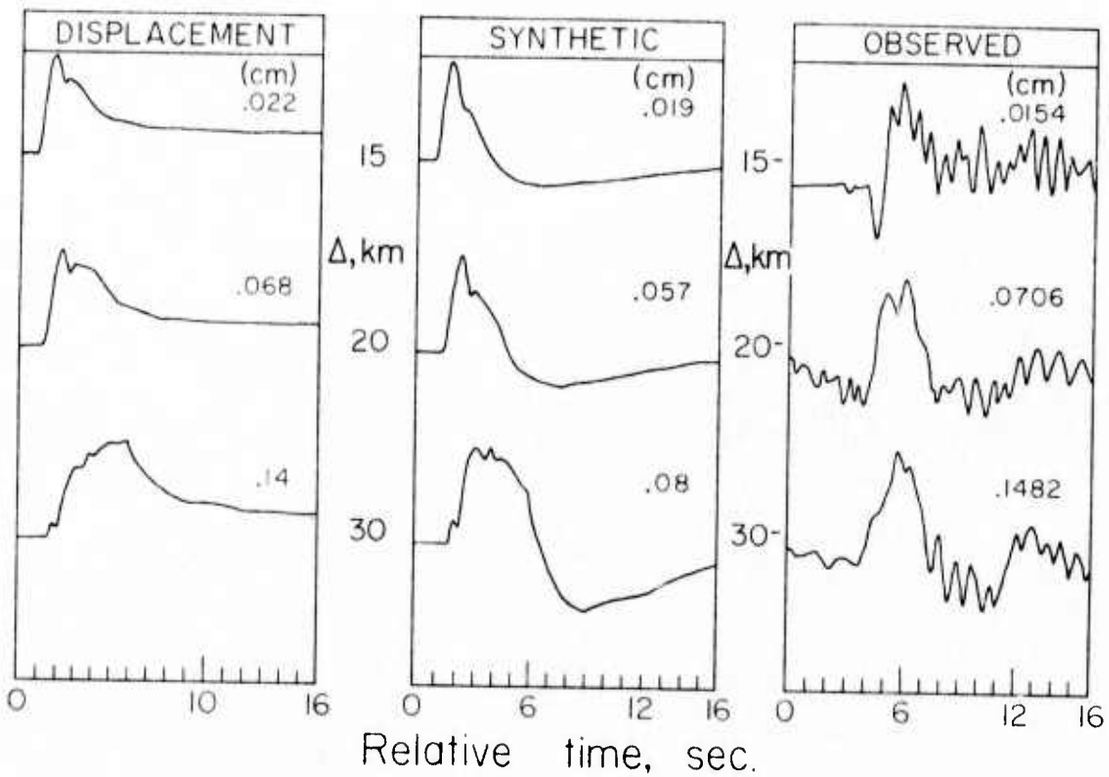

Figure 9. Comparison of synthetics with observations at SAGO-C using the source parameter given in Table 3.

and, in general, are somewhat too small at the larger ranges. Although the width of the positive pulses are about right at Δ = 15 and 20 km the synthetic at Δ = 30 km is slightly too long and the backswings are obviously too long at all stations. The latter feature will become much more obvious when we examine the spectra in the next section. However, it should be noted that at these long periods we can no longer expect our earlier hypothesis about receiver structure to hold and that the entire path is now important, thus allowing lateral refractions along the fault to become a severe problem. One would expect these observations to become progressively contaminated by lateral refractions as one moves back into the signal. This is the reason for concentrating on the beginning portion of each record.

SPECTRA

The spectral comparison of the observations with synthetics is given in Figure 10. These spectra are based on the entire wave train and since the synthetics do not contain the near-field terms we must be careful in our interpretation of the longer periods (Johnson, 1974 and Helmberger, 1974). Furthermore, our models were determined by the early portion of recordings with a disregard of everything after 15 seconds. Nevertheless, the agreement at SAGO-E is remarkably good with even some of the scalloping effects present although this is probably of minimal importance. One of the most important features of the observed spectra is the relative shift in peak values going from about .25 hz at Δ = 15 km. We interpret this effect as caused exclusively by the development of the surface waves which we feel is modeled quite well.

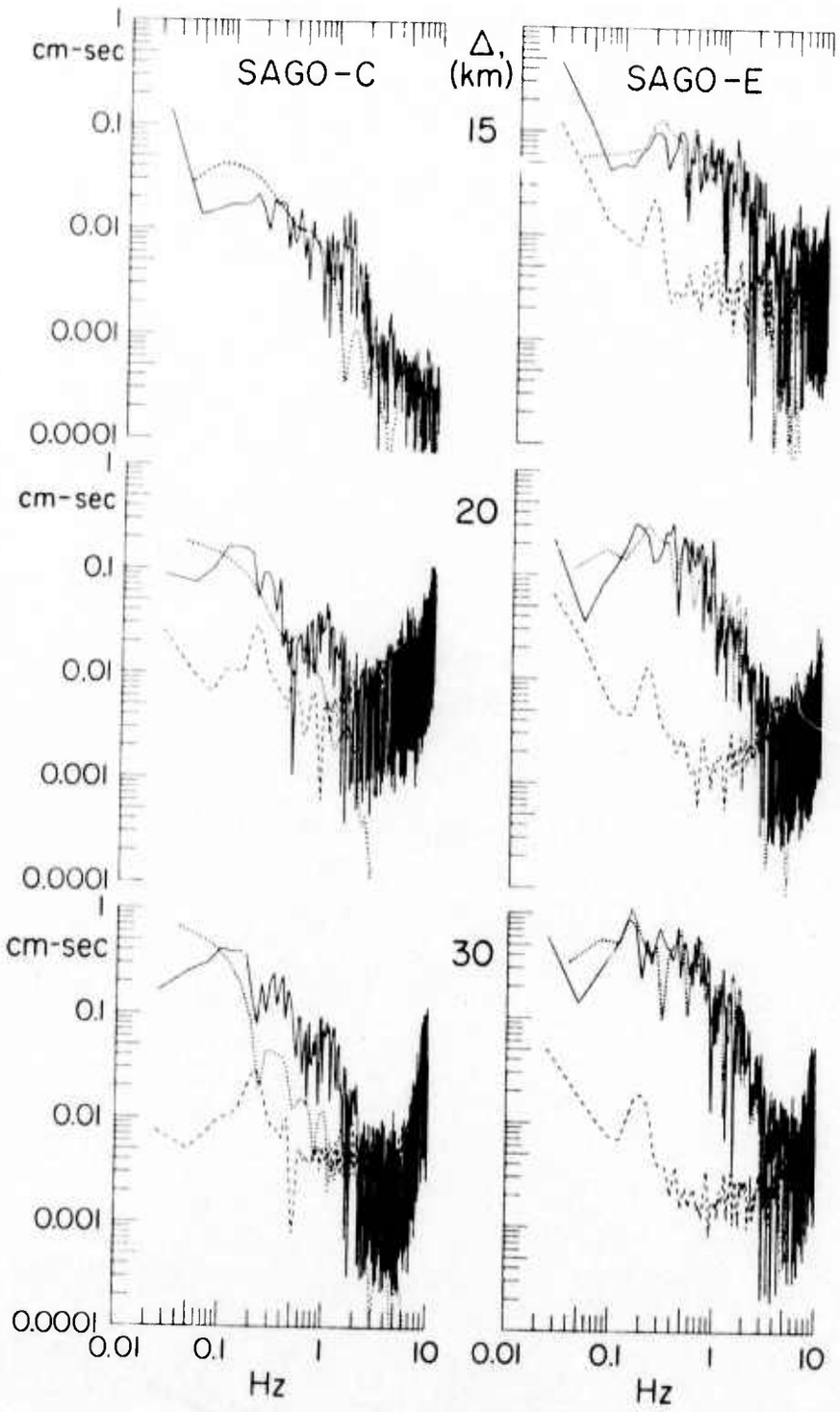

Figure 10. Amplitude density spectra of the various events with the observed given as a solid line, synthetic by a dotted line and estimates of the noise as a dashed line.

On the other hand, the agreement between synthetics and observed at SAGO-C is poor, especially at the nearest range where the long period level in the synthetics is much too strong. Of course, the reason for the strength of the long period lead for the western model as compared to the eastern model is due to the velocity difference of the bottom halfspace. This situation leaves us with a velocity contrast across the fault and if we assume the same source strength or moment than the corresponding displacements at long periods will be proportional to the ratio of the velocities cubed. Actually, the dislocation model occurring on the boundary of two different materials has not been investigated as far as the authors are aware and it is not particularly clear how to treat the relative strengths. But just changing the moment does not solve the problem. What is required is a mechanism of allowing the shorter period signal (1 to 3 secs) to come from a region of low velocity and the longer period energy to come from a region of low velocity and the longer period energy to come from a region of higher velocity. This implies a local low velocity zone near the fault but this interpretation is extremely tentative. A numerical model of a source in this type of environment would be most useful.

Another interpretation is that the faulting occurs on the eastern side of a low Q zone and that the shorter periods are either absorbed or scattered in route to SAGO-C. However, Johnson and McEvilly (1974) do not report on any such low-Q zones although this condition is hard to dismiss.

DISCUSSION

The observations examined in this study are probably too near the fault zone to obtain highly accurate estimates of the source parameters although SAGO-E seems explicable. Nevertheless, it is interesting to compare various size earthquakes that have been studied in the time domain with adequate corrections for earth structure. For convenience, we will define duration,

$$\tau = \frac{1}{2}\,\delta t_1 + \delta t_2 + \frac{1}{2}\,\delta t_3$$

and a corresponding corner frequency, $f_o = 1./(\pi\tau)$, after Helmberger and Malone (1975). The results, displayed in Figure 10, for the three events discussed earlier are supplemented by events 1, 2, and 7a modeled by Johnson and McEvilly (1975) and the Morgan Hill event studied by Helmberger and Malone (1975). At the larger magnitudes we included three events that have been modeled at teleseismic distances. These latter events have been modeled by inverting to long-period waveforms containing the main crustal phases P, pP, and sP and similarly for the S phases. The detailed information about fault orientation, depth, and source time duration are obtained by using the azimuthal coverage. Lines of constant stress drops are included for comparison although the actual level is rather arbitrary; that is, the stress drop is defined by

$$\Delta T = (7/16)\, M_o / r^3$$

after Keilis-Borok (1960) for a circular fault surface with r = radius with estimates of

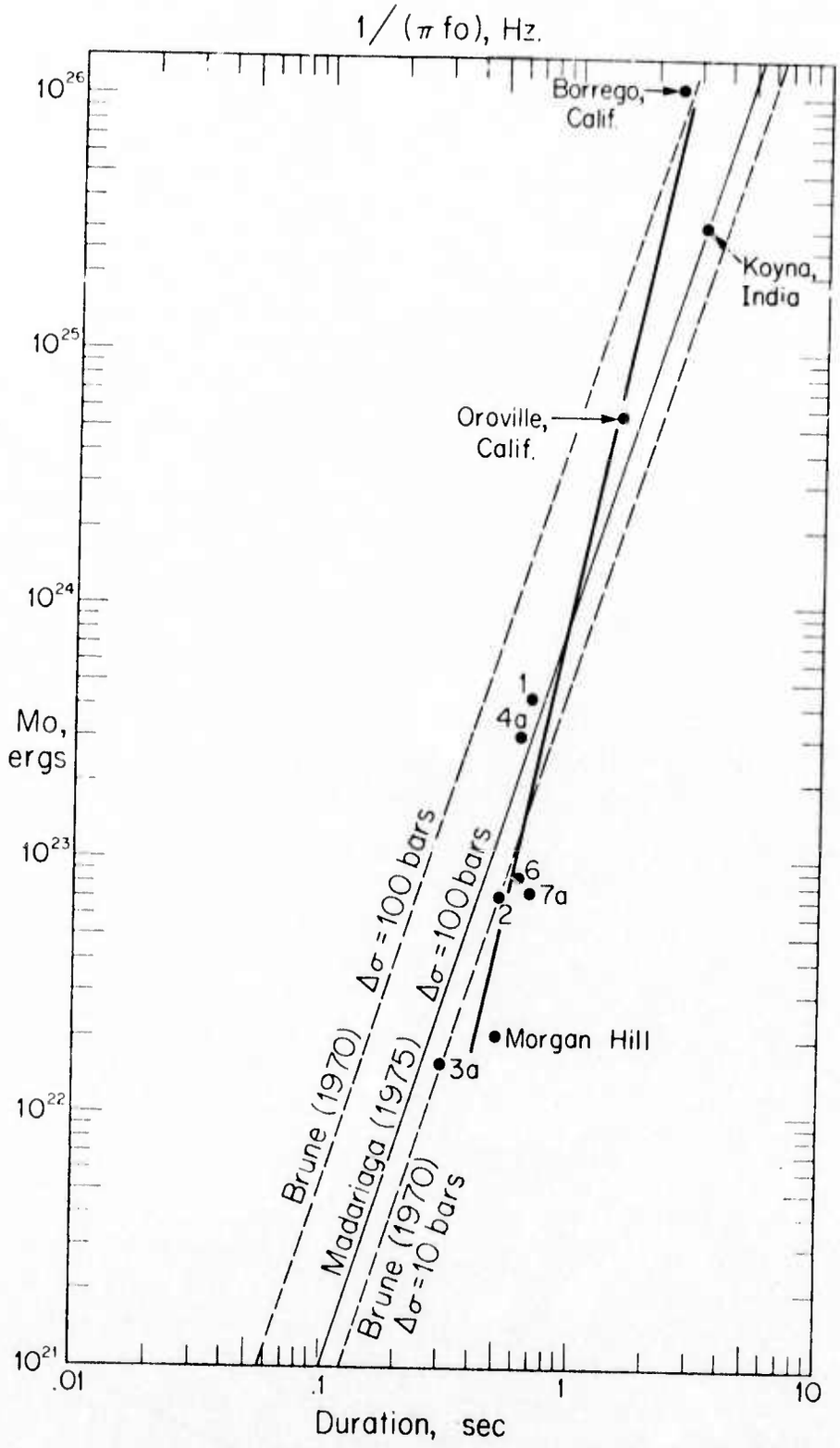

Figure 11. Duration versus moment plot for the various events determined by fitting observations in the time domain. The data for the larger events are taken from Langston and Butler (1976) (Oroville), Langston (1976) (Koyna), and Burdick and Mellman (1976) (Borrego).

$$r = 3.5\ \beta/f_o \quad \text{(Brune, 1960)}$$

and

$$r = .21\ \beta/f_o \quad \text{(Madariage, 1975)}.$$

Accurate determinations of r independent of f_o have not been made although a number of experiments are presently designed for this purpose.

The trend at these points suggest that the larger events have higher stress drops than the smaller events at least for the California events although the data selection may be biased in that the only broad-band data available in the M_L = 4 to 5 range comes from the Bear Valley region. It might also be argued that the Borrego and Oroville events may not be representative and that many more events must be considered before a definitive conclusion can be reached especially events in the M_L = 5.5 range. The latter size is near the threshold of allowing body wave studies at ranges 15 to 30 degrees where the nature magnification caused by the upper mantle structure can be used to advantage; such studies are now in progress.

A meaningful relationship between duration versus moment is not only important with respect to learning something about the stress conditions in the earth but it is essential to estimating strong ground motion for a given earthquake with a specified moment. We are suggesting that under ideal conditions ground motion amplitudes at periods .1 to 10 seconds can be predicted if we know the source parameters namely moment, orientation, depth, and source duration, and if we know the receiver crustal response. The fault orientation and depth are of key importance in such predictions as demonstrated by Johnson and Helmberger (1976).

In summary, the broad direction of this paper has been to address the problem of separating effects due to structure as opposed to source derived by using recent developments in the methods of synthesizing motion in a layered halfspace. Within this framework, a comparative analysis of the calculated and observed ground motions for several earthquakes were performed at two vastly different sites with respect to surface geology. Our results suggest that the beginning portion of local seismograms can be profoundly altered by the upper-crustal structure. This means that the seismogram contains prominent periodicities many of which are only weakly related to source radiation and, in fact, are more strongly related to the receiver structure. Once the receiver structure is known, or a transfer function determined which is a weaker condition, we become one step closer to estimating local ground motions for future events as well as learning something more about local geology.

TABLE 1

Data Summary

Event Number	M_L	SAGO-C Depth (km)	SAGO-C Dist (km)	SAGO-C Az deg	SAGO-E Dist (km)	SAGO-E Az deg
3a	4.0	3.7	13.2	311	14.8	334
4a	5.1	6.4	29.7	311	30.7	322
6	4.7	5.1	21.3	310	22.4	325

TABLE 2

Upper-Crustal Models

Model	Layer No.	Thickness (km)	Velocity (km/sec)	Density (gr/cm^3)
E	1	.35	.75	1.5
	2	1.95	1.80	2.2
	3	∞	3.3	2.6
W	1	.75	3.5	2.7
	2	1.75	2.7	2.6
	3	∞	2.0	2.6

TABLE 3

Source Parameters

Event Number	M_L	Moment (dyne-cm)	Source Duration (sec)
3a	4.0	1.6×10^{22}	.3
4a	5.1	3.1×10^{23}	.6
6	4.7	8.9×10^{22}	.6

III. INVERSION OF THE BODY WAVES FROM THE BORREGO MOUNTAIN EARTHQUAKE TO THE SOURCE MECHANISM

Since the introduction of simple theoretical fault models, many investigators have attempted to infer details of earthquake faulting by comparing far field body wave recordings with model predictions. They have found that most deep and intermediate events have simple waveshapes which can be easily explained with smooth dislocation models, (Mikumo, 1971, a, b, Teng and Ben Menaham, 1965, Burdick and Helmberger, 1974) but that shallow earthquakes have very complex waveforms. Until recently, this was interpreted to mean that shallow events have fundamentally more complex fault surfaces and time histories. By determining the response of a layered halfspace to a shallow double couple point source, Helmberger (1974), Fukao (1971) and Hudson (1969), among others, have shown that this interpretation is not entirely correct because much of the waveform complexity is caused by the interaction of the source with the free surface. Thus, it will once again be worthwhile to address the question of whether or not a smooth dislocation is appropriate for shallow earthquakes. This time, however, the free surface interaction should be included in the analysis.

Many of the previous investigators of body waves from shallow

events have focused their attention on the fourier transform of the entire body wave pulse. They employed a technique which enabled them to determine important source parameters such as seismic moment, stress drop and source dimensions from the rough characteristics of the amplitude spectrum (Hanks and Wyss, 1972, Wyss and Hanks, 1972,a,b, Molnar and Wyss, 1972, Molnar, Tucker and Brune, 1973). Since reflected or converted phases such as pP , sP or sS can affect both the long period level and the shape of the amplitude spectrum, it will be important to see if the results change when the free surface is correctly accounted for.

Langston and Helmberger (1975) have outlined a simple procedure for including the surface interaction in the computation of a synthetic seismogram from a model of a shallow dislocation source. In other words, they have presented a tractable solution to the forward problem of computing the data given the model. We have demonstrated in a related work (Mellman and Burdick, 1976), that the existence of a solution to the forward problem along with a quantitative method for comparing the synthetic to the actual data make it possible to solve the inverse problem; that is, an optimal fault model can be determined from the data by an iterative generalized linear inverse technique. We present here the result of the application of the inversion technique to the Borrego Mountain earthquake of April 9, 1968. We present a final model which accurately predicts all of the observed waveforms. We then use the model to identify a single, strong arrival in the record, and finally we interpret the shape of this basic seismic pulse in terms of a smooth dislocation model.

THE BORREGO MOUNTAIN EARTHQUAKE

The Borrego Mountain event was a magnitude 6.4 strike slip earthquake which occurred at 2:29 G. M. T. April 9, 1968 on the Coyote Creek fault in southern California. Figure 1 shows the location of the main shock as well as many of the aftershocks and the trace of the ground breakage. After the event, both the California Institute of Technology and the USGS undertook a thorough study of all major types of postseismic phenomena. From their observations, we can draw two important conclusions which bear heavily on our interpretation of what happened during the earthquake. The first is that even though the ground breakage appears simple, the pattern of stress release was probably very complex. This can be inferred from the following points: (1) In the Imperial Valley, the San Andreas fault splays out into a number of closely interrelated faults. Each nearby zone of weakness contributes to the complexity of the stress pattern near the Coyote Creek fault (Sharp, 1972). (2) Surface offsets were observed on the Imperial, Superstition Hills and San Andreas faults as well as the Coyote Creek fault (Allen et.al. 1972). (3) The aftershocks had a very diffuse spatial pattern. It defined only a broad three dimensional region of stress release instead of a single plane of failure (Allen and Nordquist, 1972, Hamilton, 1972). This complex prestress pattern seems to manifest itself in some unusual aftershocks occurring immediately after the main shock.

The second conclusion which can be made from the postseismic observations is that there was a clear difference in the behavior of the north break (segment BC in figure 1) and the south break

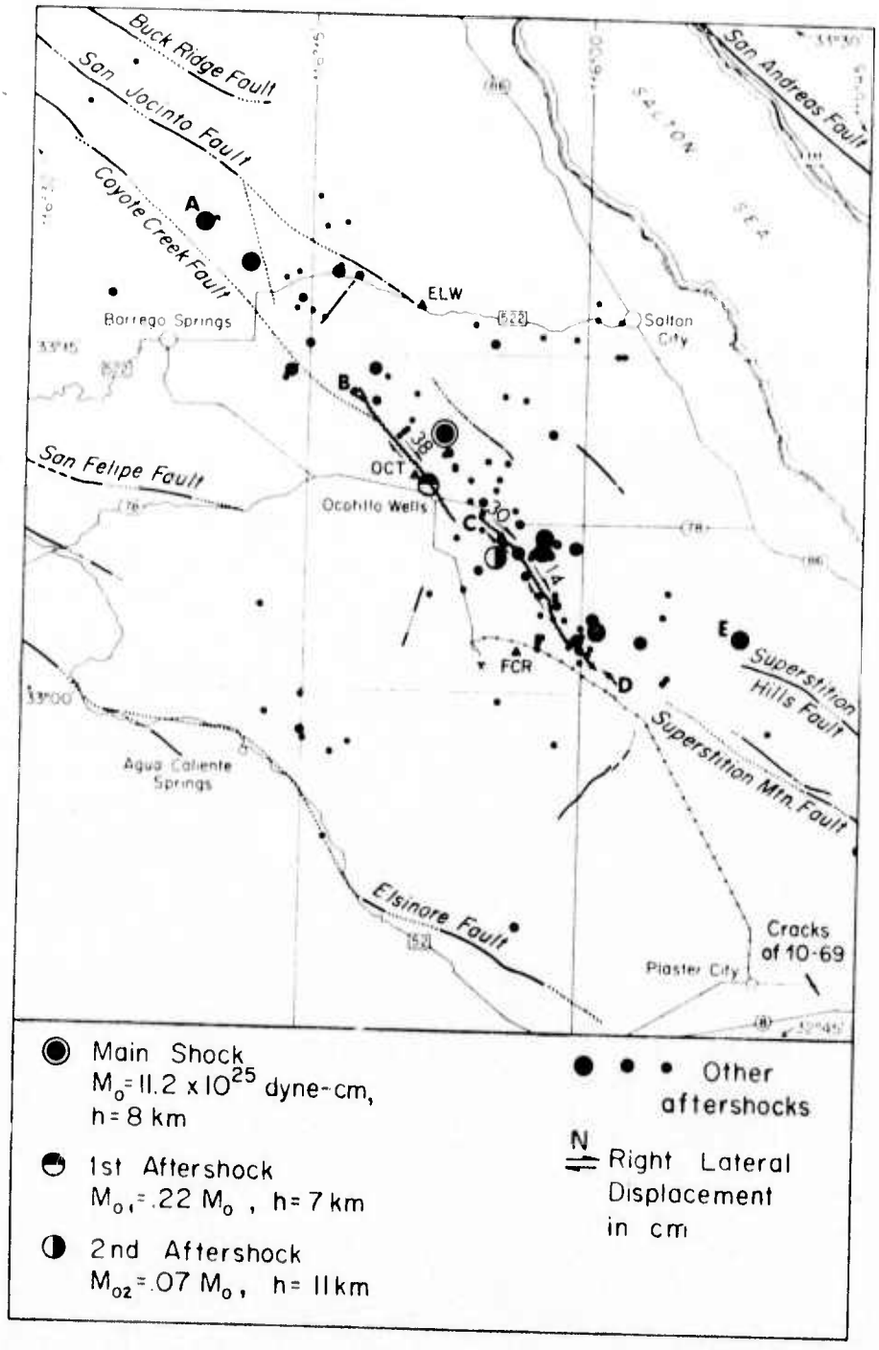

Figure 1. The Borrego Mountain Tectonic Zone: Segment AE ~55km marks the extent of the aftershock zone and BD ~31 km the total rupture length. Segment BC radiated most of the energy in the main shock. The length of this segment plus the 8 km depth of the main shock motivated the choice of a circular fault model with radius 8 km. Segment CD~17 km was probably due to a swarm type event. (Figures 1 and 2 modified from Allen and Nordquist, 1972).

(segment CD in figure 1). The north break had a large initial surface offset, relatively few aftershocks and very little postseismic creep. The south segment had a small initial offset, more aftershocks, and as much postseismic as coseismic displacement (Allen and Nordquist, 1972, Clark, 1972, Burford, 1972). Evidence in the body waves shows that these variations reflect different behaviors deep in the earth.

THE DATA SET

The data set used in the inversion procedure was selected from the P and SH body waveforms recorded at stations in the World Wide Seismograph Station Network. Recordings made outside the epicentral range of 30 to 90 degrees were excluded to circumvent problems with upper mantle or core structure, and recordings with a signal to noise ratio of less than 5:1 were excluded to reduce difficulty with background noise. Processing noise was kept to a minimum by digitizing each record ten times and averaging the results. The names and locations of the stations which had records of acceptable quality are listed in table 1 and their azimuthal spread shown in figure 2. The stations are plotted along with the first motion data and the fault planes determined by Allen and Nordquist (1972). It is regrettable that no high quality waveform data was available to the southwest of the event but there was sufficient coverage to impose some heavy constraints on the allowable source mechanism. The observed waveforms are the top traces shown in figure 5.

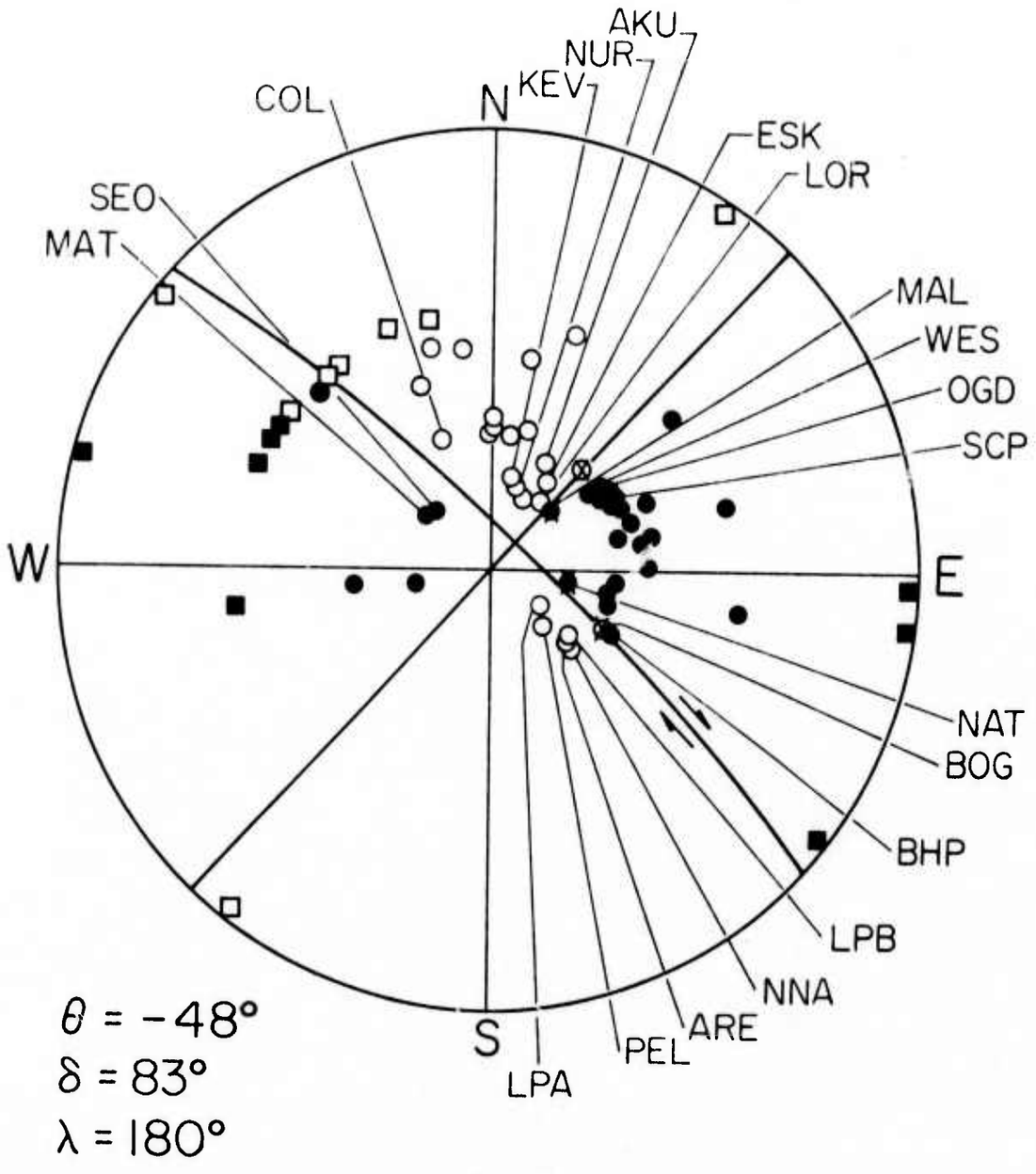

Figure 2. The stations used in this study as they distribute with respect to the fault plane solution determined by Allen and Nordquist (1972). Unlabeled points are other stations which they used in their first motion study. θ is the fault strike, δ the dip and λ the rake.

MODEL PARAMETERIZATION AND INVERSION

The first step in applying linear inversion theory to a problem is to formulate a technique for computing theoretical values for the observed data from a finite number of model parameters. In the Langston and Helmberger (1975) procedure for computing synthetic seismograms for a point dislocation source, the basic parameters are a time function, source depth and the three fault orientation parameters. If the source is to be considered as a sum of point sources, the same parameters as well as a relative size, time and location must be specified for each additional source. The origin time and epicentral location of the primary source are assumed to be known quantities, and its absolute size need not be specified if only relative waveshapes are considered. In order to obtain an adequate fit to the Borrego Mountain data, it was necessary to use a sum of three sources. This made a total of 20 parameters and three time functions which had to be specified to compute the synthetics.

The problem of parameterizing a time function can be approached in two ways. The first is to directly parameterize some pulselike function and assume that it is independant of azimuth. The second is to use a finite source model. The free parameters in a finite source are usually the rupture velocity and average dislocation time on a failure surface with some assumed geometry. The time pulse for such a model is a function of both azimuth and take off angle (Fukao, 1971, Savage, 1966). The approach used in this study was to begin with a simple, azimuthally independant pulse. After an optimal model was obtained, the synthetics were

compared with the data to test for any evidence which might justify an azimuthally dependant model. The azimuthally independent pulse shape chosen was a triangular pulse requiring only two parameters; a zero to peak time and a peak to zero time.

It was also necessary at the outset of the inversion procedure to choose a near source and near receiver earth structure. Again the decision was made to start with the simplest possible assumptions, but to continuously test for any features in the data which would justify a more complex model. More specifically, at the beginning only the rays P, pP and sP (or S and sS) were computed. At several points, however, the strongest rays generated by the near source structure proposed by Hamilton (1972) and the near receiver structure discussed by Burdick and Helmberger (1974) were also included. No effects which could be unambiguously attributed to layered structure near the source or receiver were ever identified, so throughout this study only the five basic rays were used to compute the synthetics.

Once the model had been parameterized, it was necessary to define some quantitative measure of the correctness of a given model. This was done by first defining the correlation between a computed seismogram $S_i(t)$ and an actual seismogram $d_i(t)$ as

$$N_i = \text{Max} \left[\int_o^T S_i(t)\, d_i(t + \tau)\, dt \right]$$

where $$\int_o^T S_i(t)^2 dt = \int_o^T d_i(t)^2 dt = 1$$

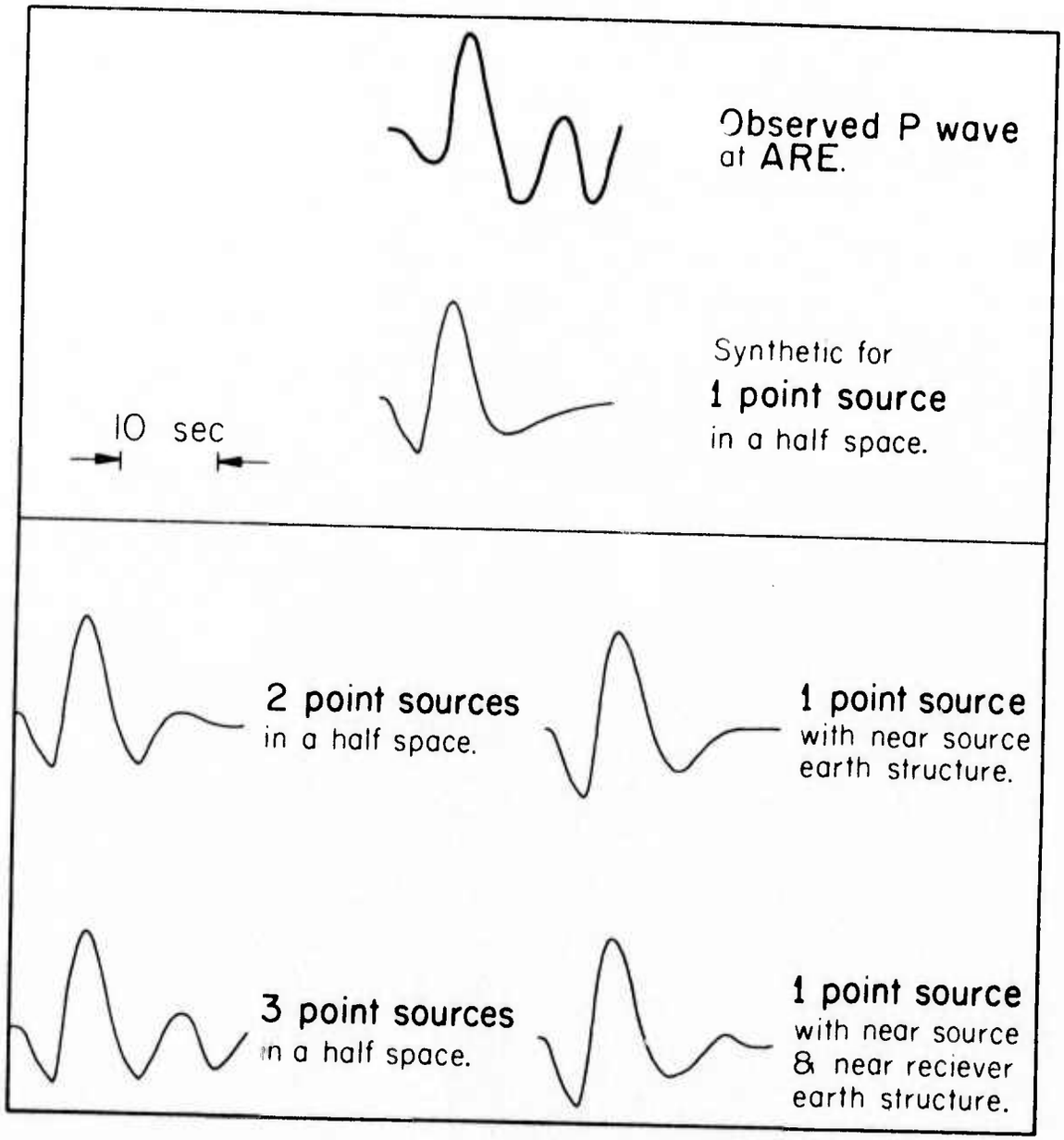

Figure 3. The top of the figure shows that a single point source can not account for the structure late in the seismogram. The left volumn shows that it is possible to obtain a better fit by adding in additional point sources while the right shows that inclusion of the rays generated by the near source crustal structure (Hamilton, 1972) and an appropriate near receiver structure does not.

T is the window length which in this case was 25 seconds, and i is an index which ranged over the data set. The repeated index does not indicate a summation. The total measure of model correctness M was given by

$$M = \sum_i (1 - N_i)^2$$

Since N_i uniquely approaches 1 when S_i approaches d_i, M goes to zero when the synthetics match the data exactly. The derivatives of M with respect to the model parameters were taken numerically and linear inversion technique applied to find an optimal model (Mellman and Burdick, 1976).

The initial attempts at inversion were made using a single point source model. The top two traces of figure 3 illustrate the result for a typical seismogram. It was clear that, although the model was adequate for the first few seconds, there was much more structure present in the later portion of the seismogram than was predicted by the synthetic. This could have been the result of either a complicated earth structure or a more complicated source mechanism. On the right in the third row of figure 3 is shown the synthetic including the effects of assuming that the Hamilton (1972) crust model exists near the source, and on the left is the result of including a second point source. In the lowest row, the result of including three point sources is shown as opposed to including both the near source and near receiver crustal effects. (see Table 2) The effects of introducing appropriate earth structure were always too small to explain the discrepancies between the synthetics for

a one source model and the observations. We concluded that the structure late in the waveforms was probably caused by the first large aftershocks. We attempted to model the first two with additional point sources.

The previously published mechanism for the Borrego main shock was used as a starting model for the single point source inversion runs. When it became apparent that a multiple point source model would be necessary, the seismograms were examined to determine the time when the data first began to diverge from its predicted behavior. A new point source was postulated to have occurred at that time. It was initially presumed to have had the same location as the main shock. The space of possible fault plane solutions for the second source was then explored by trial and error using a crude spacing between models. Synthetics were computed for only a few key observations. When a roughly satisfactory model had been determined, the inversion procedure was used to iterate in on a more refined model for the location, time, time function and fault plane solution of the shock. The same procedure was used on the second aftershock. We stress that there can be no way of insuring that the models found by this method are in any way unique. However, as we shall show, they do predict the fine details of the observed waveforms very closely. Also, we can state that in our rough search of the model space we did not find any other model which came nearly as close to predicting the data as the one presented in the following section.

THE FINAL MODEL

In the second row of figure 5 are the synthetic waveforms for the final model. Those arrivals which are marked are the direct arrivals and the primary reflections from the main shock. The later complications in the waveform are caused by the later shocks. The wide variety in the appearance of the secondary structure provides an additional indication that it is a manifestation of source and not crustal complexity. A strong arrival from a sharp layer always arrives at nearly the same point on the record and generally varies slowly as a function of azimuth. But a secondary source predicts three arrivals, P, pP, and sP whose interaction can vary rapidly with azimuth. The final source locations, time functions and fault planes used in computing the synthetics are shown in figures 1 and 4.

Given that structure generated arrivals on the order of those shown in figure 3 have been neglected, the fit to the data appears most satisfactory. For each peak in the data, there is a corresponding peak of the right duration and sign in the synthetics. The worst fits both in terms of visual appearance and the correlation N_i occur for the P waveforms at stations where P and pP arrive with the same polarity. These include MAT, SEO, LPB, ARE and NNA. Their common feature is that they lie off the

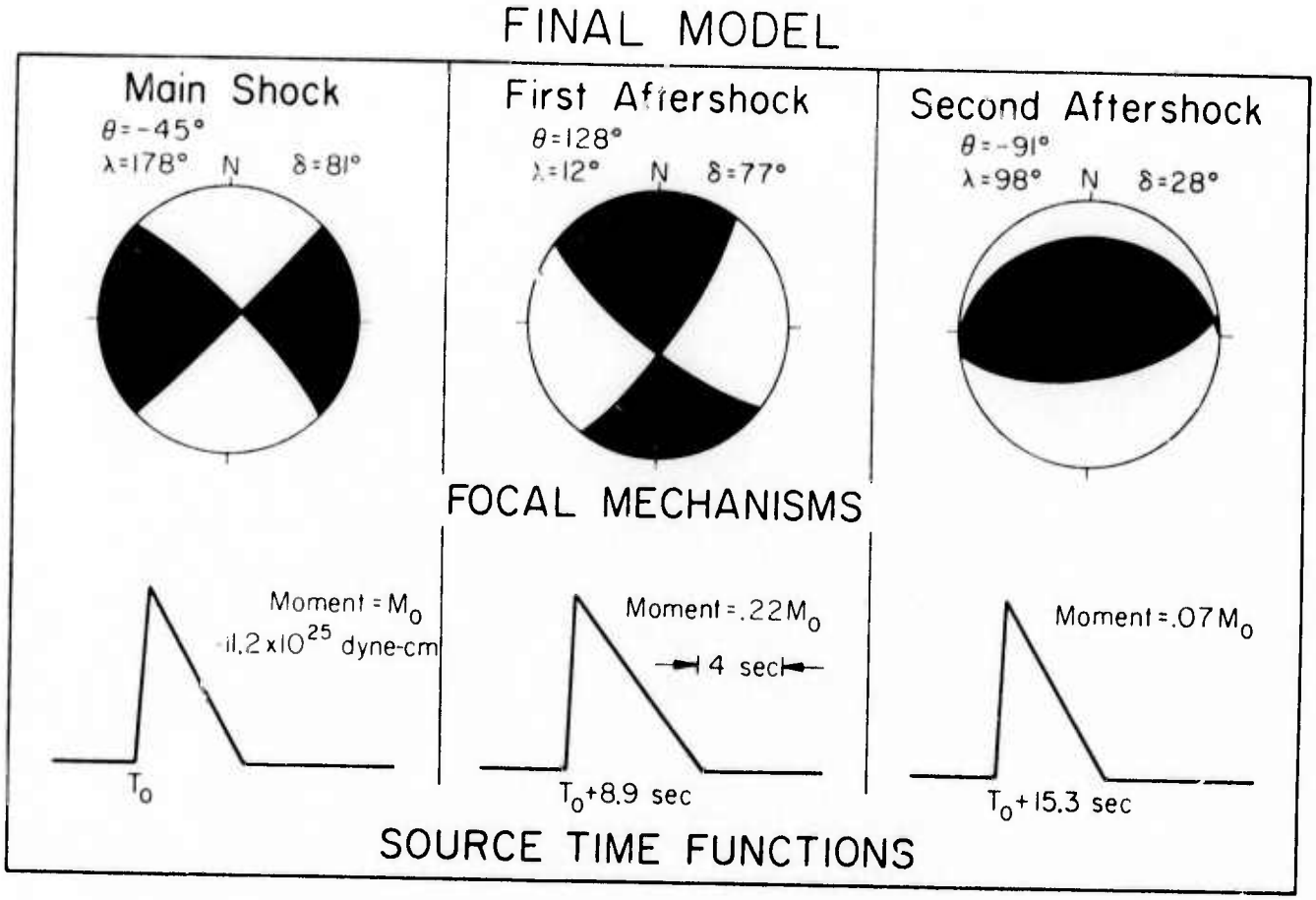

Figure 4. The fault plane solutions and the time functions of the main shock and the first two aftershocks. The shaded portions of the circles represent the compressional quadrants. The fault orientation parameters have been defined in Langston and Helmberger (1975).

very ends of the fault trace. They are composed of rays which travel directly along the fault plane (see Figure 2). As Figure 5 shows, the difficulty is that the predicted ratio of the peaks $sP/(P + pP)$ is too small with respect to the observed values. There is no way to determine whether this occurs because of anomalously large S or anomalously small $(P + pP)$ without the use of absolute amplitude measurements.

A value for M_o, the seismic moment of the first source, can be determined from a measurement of the absolute amplitude at each station by use of the formula

$$M_o = \frac{A \text{ observed}}{A_1}$$

A observed is the observed amplitude of either the sP or the S +sS peak and A_1 is the theoretical amplitude of the same peak for an event with moment one. The moment values determined from the twenty eight observations used in the inversion are listed in table 1. They have an average value of 11.2×10^{25} dyne-cm and a standard deviation of 2.8×10^{25} dyne-cm. The relative errors between the amplitude computed assuming the average moment and the observed amplitude are plotted against an azimuthal angle ϕ in Figure 6. This angle is defined to be zero for stations directly off either end of the fault and to have a maximal value of 90° for stations in a direction perpendicular to the fault. The observed values of sP tend to be too large and the observed values of S + sS too low whenever those rays travel directly along the fault zone. It

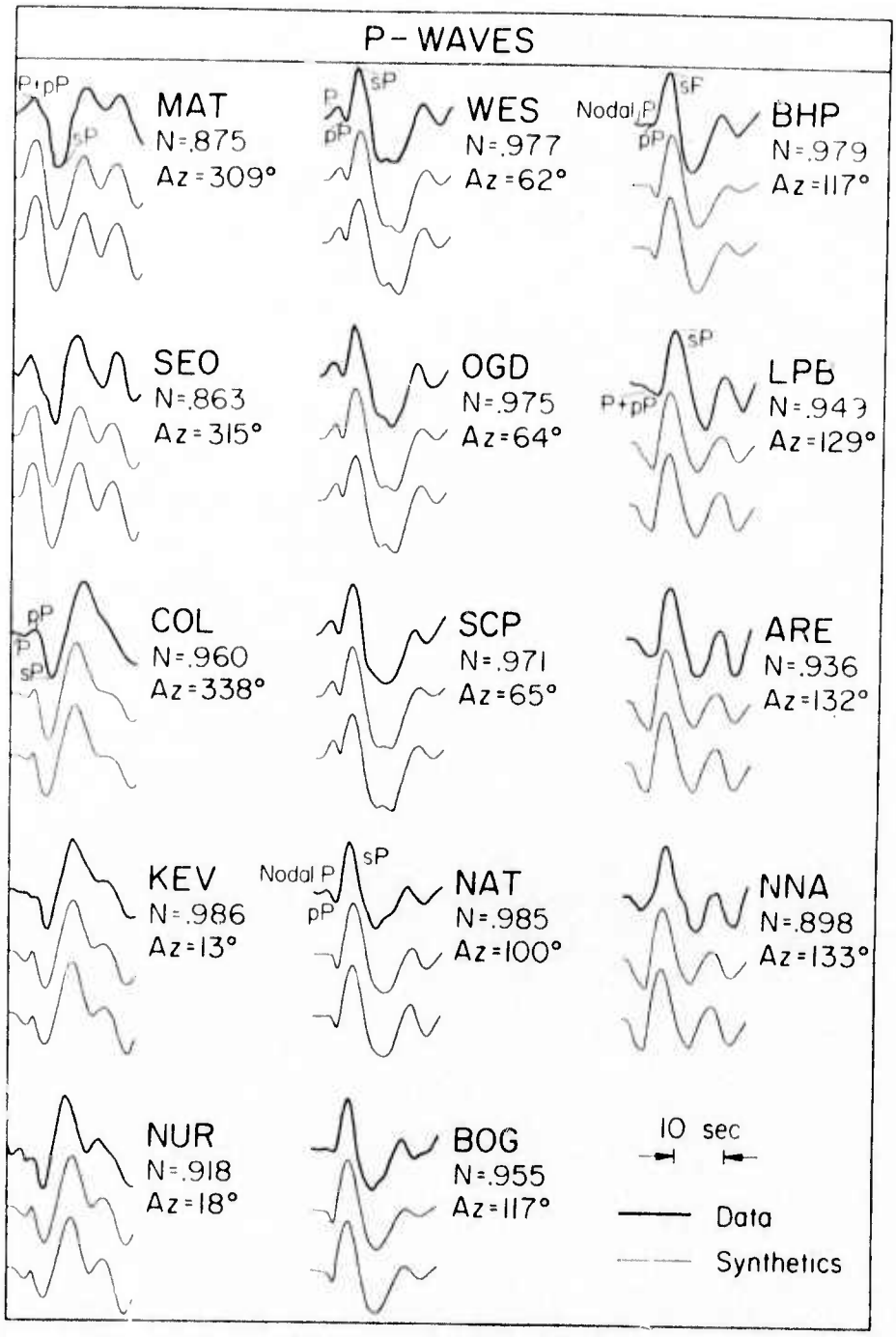

Figure 5a. The observed P waves (top) predicted by the final (3 point sources with azimthally independant time functions) model (middle) and the synthetics predicted by the same model with the main shock represented by a finite (azimuthally dependant time function) source model (bottom). The quantity Ni is the normalized correlation operator which uniquely approaches 1 as the synthetic approaches the data. The azimuthes are measured from North.

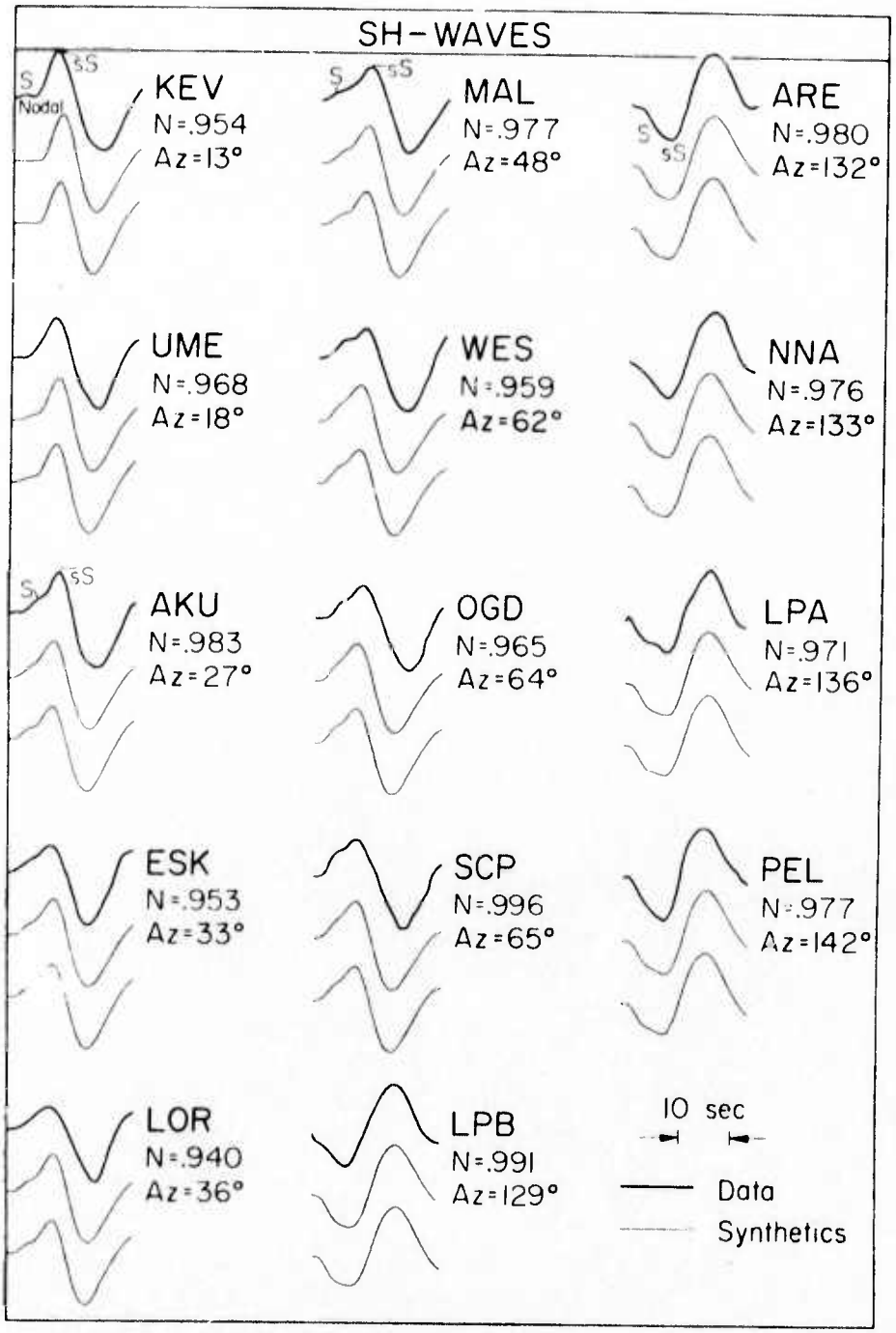

Figure 5b. The observed SH waves (top) predicted by the final model (middle) and the synthetics predicted by the same model with the main shock replaced by a finite source model. The labeled arrivals in both Figure 5a and Figure 5b are from the main shock. In both figures, the stations are shown in order of increasing azimuthal deviation from the NW extension of the fault trace. (see Figure 2)

is important to note that most of the tectonic features in the region also trend parallel to the fault. The implication is that the ratio of the amplitudes of SV to SH is sensitive to the lateral variations induced by the fault itself or by some other tectonic feature. Since the sP phase is often the dominant one in the far field P waveform, this instability may be responsible for anomalies in P waveshape and amplitude as well as in the S.

The fault plane determined for the main shock (Figure 4) is virtually identical to the one determined from the first motions data by Allen and Nordquist (1974). The strike of the northwest trending plane corresponds closely with the strike of ground breakage, and the motion indicated by the conjugate plane corresponds with most of the observed offsets. There can be little doubt that the northwest plane is highly representative of the actual plane of failure. Because of the information in the body waves about the separation of P, sP and pP, the depth can be constrained to be between 7 and 9 kilometers.

The second shock was apparently a left lateral, strike slip event occurring 9 seconds after the first. The location is very poorly constrained, since it did not occur far enough away from the main shock to cause obvious azimuthal dependance in its arrival time (Figure 1). As shown in Figure 4, it seems to have released a stress nearly reversed to that of the main shock. There are several indications from other types of data that such an event might have occurred. First, there were observations of ground displacement near point B with a left lateral component which was clearly not of the Reidel type (Clark, 1972). Second, there are the previously cited lines of evidence which suggest complex prestress and stress release patterns in which reversed stresses might easily have developed. Sharp (1972) mentions several instances where left lateral strain buildup had been reported in the region in the past. Finally, studies by Burridge (1969) and Madariaga (1975) have shown that it is theoretically possible for reversed or overshoot type stresses to develop even in relatively simple cases.

The third shock which occurred approximately fifteen seconds after the first was a thrust event (Figure 4). This mechanism is consistent with the stress pattern which induced the first event in that the major axis of compression is roughly similar. The location is again very poorly constrained by the far field data, but it appears that the shock occurred near point C in Figure 1. The surface break takes a sudden step to the left and shows an abrupt decrease in total offset at this point. Also, one of the later aftershocks which occurred there was a thrust event with a mechanism similar to this one (Hamilton, 1972). These are the first of several correlations that were found between details of the postseismic observations and the final source model. The second shock had a moment only a quarter as large as the first and the third less than a tenth of the first. Since they were much smaller, they had a relatively minor effect on the waveform and on the surface break. In effect, they are nothing more than the first and second aftershocks. The first event which radiated the most energy determined the first motions and the gross features of both the waveforms and the ground breakage.

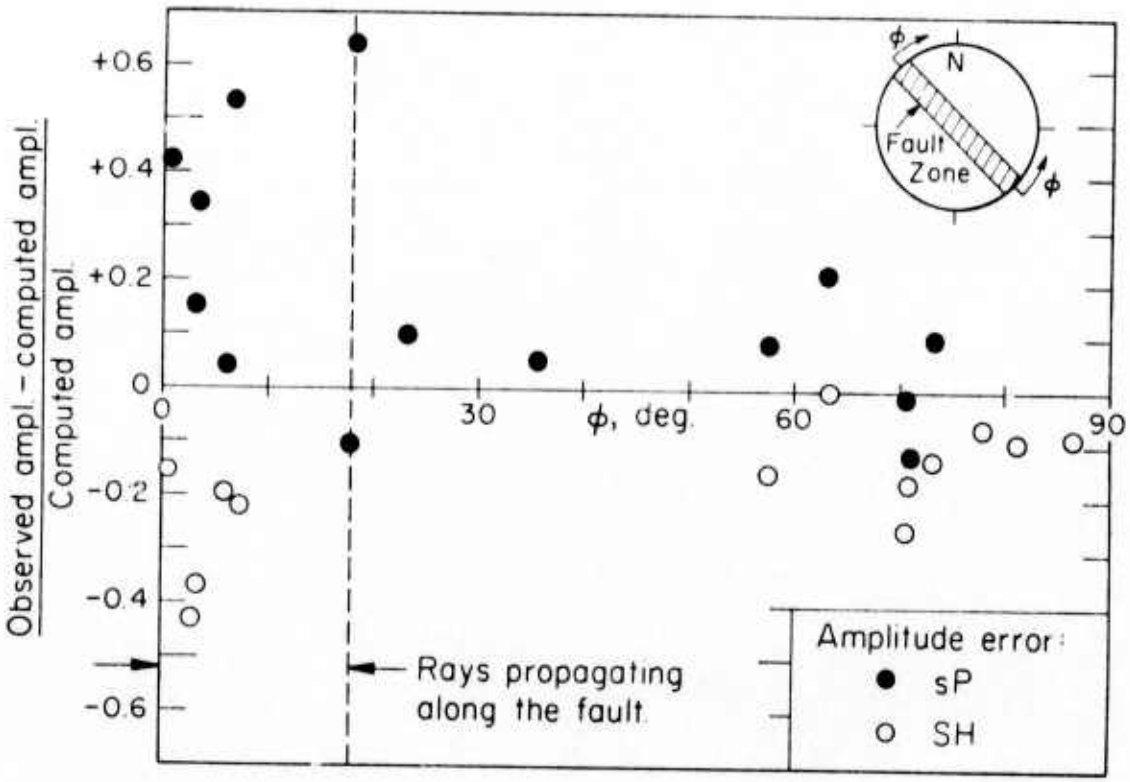

Figure 6. The dependance of the scatter in the amplitude data on the azimuthal angle ϕ which is defined so that it becomes small whenever rays propagate along the fault zone. The final model can predict observed amplitudes to within 25% except at stations with low values of ϕ.

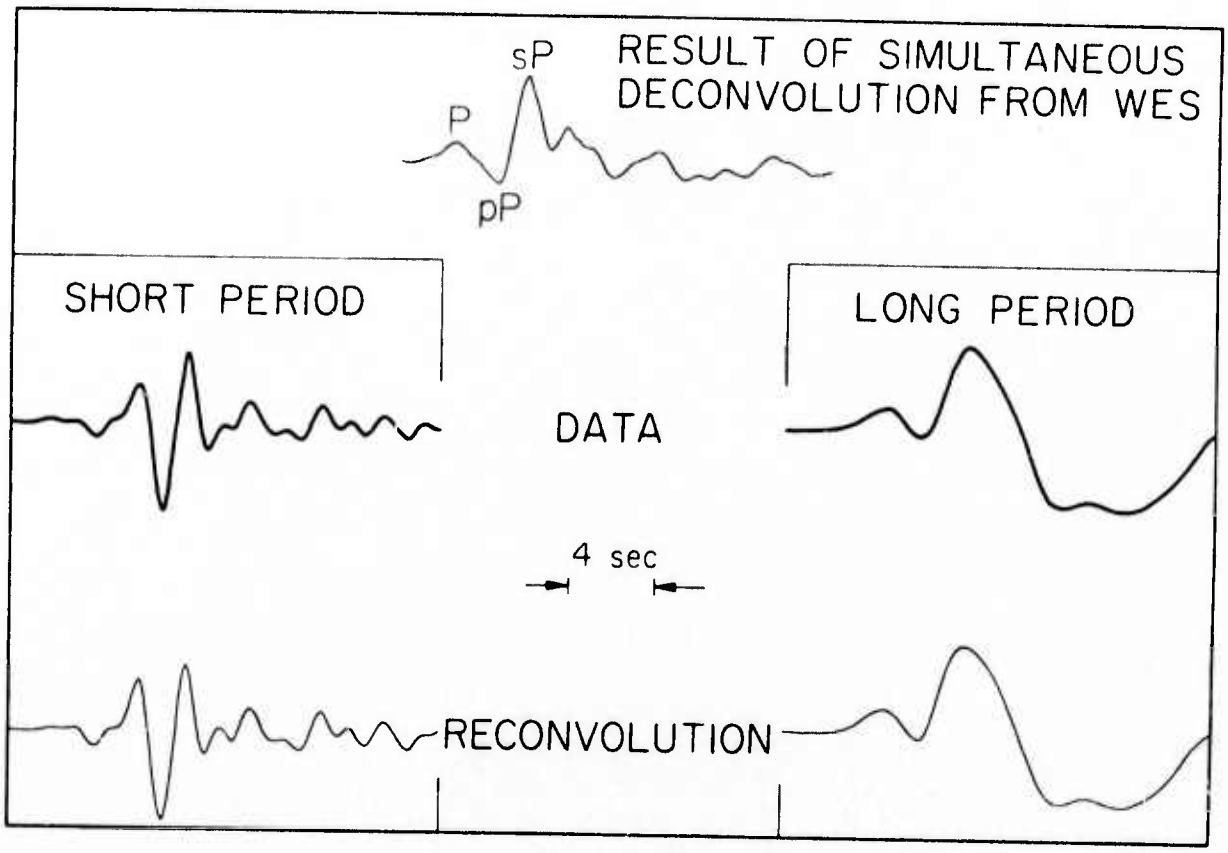

Figure 7. (Top) A time function which is compatible with both the long period and short period records from WES. It was obtained by fourier transforming both records (middle traces), dividing out the instrument and Q filter from each, taking a weighted average of the results and inverse transforming. When the top trace is reconvolved with the appropriate instrument and Q it produces the bottom traces.

A FINITE SOURCE MODEL

We return now to the initial question of what type of finite source model is appropriate for shallow earthquakes. We will attempt to model the first source since it was the largest. Figure 5 shows that it would be difficult to separate the direct P pulse from the pP or the S from the sS. The sP, however, is strong enough to be relatively clear on the record. We present here an attempt to determine a model which fits the characteristics of that one phase. Then we use the model to compute the complete seismograms for comparisons with the data and the inversion result.

Several different techniques were used to attempt to find azimuthal dependance in the duration of the sP pulse as was done for P waves from deep earthquakes by Mikumo (1971 a, b) No clear azimuthal pattern was resolved by any of these means. The effect is apparently too small to be seen over the noise level. Any inferences to be made about the finiteness of the source will have to come from the shape or frequency content of the time function. This type of analysis requires a better estimate of the shape of the source time function than the crude result from the inversion. A much better determination was obtained by making use of the high quality recording from WES. At this station, both the long and short period recordings were strong, clear and virtually free of noise. As illustrated in Figure 7, a time function was obtained by a simultaneous deconvolution technique which could be reconvolved with either the short or long period instrument to reproduce the data.

The deconvolution technique consists of transforming equivalent segments of the long period and short period records into the frequency domain, dividing each by the appropriate instrument and Q responses, weighting, averaging and inverse transforming. The weighting function for the long period instrument was equal to one for frequencies less than .25 cps, and it fell off linearly from that frequency to zero at .5 cps. The short period weighting function was just one minus the long period function.

The portion of the deconvolved time function which is dominated by the first source sP is compared with the inversion result in Figure 8.

The deconvolution result bears a strong resemblence to the time function for a circular fault published by Savage (1966). The third trace in Figure 8 is the theoretical time function for a circular rupture propagating on the fault plane at 2.8 km/sec (.8β) to a final radius of 8 km. The dislocation - time history is assumed to be a step and the final offset is assumed to die off as $(1 - (\frac{r}{R})^2)^{1/2}$. Figure 1 shows that this would correspond to a rupture beginning at the hypocenter, propagating up to the surface, and downward by an equal amount, northwest to point B and southeast only to point C. The time function for an ellipsoidal fault surface extending all the way down to point D is too long in duration to be compatible with the inversion or deconvolution result as shown at the bottom of Figure 8. The implication is that segment CD did not contribute significantly to the energy in the body wave pulse. If the rupture velocity had been assumed to be β instead if .8β the fault radius would only have had to be increased to 9 km to keep the pulse duration the same. Therefore, this result is not dependant on the assumed rupture velocity. There is abundant evidence in the postseismic observations that the two segments behaved in different fashions.

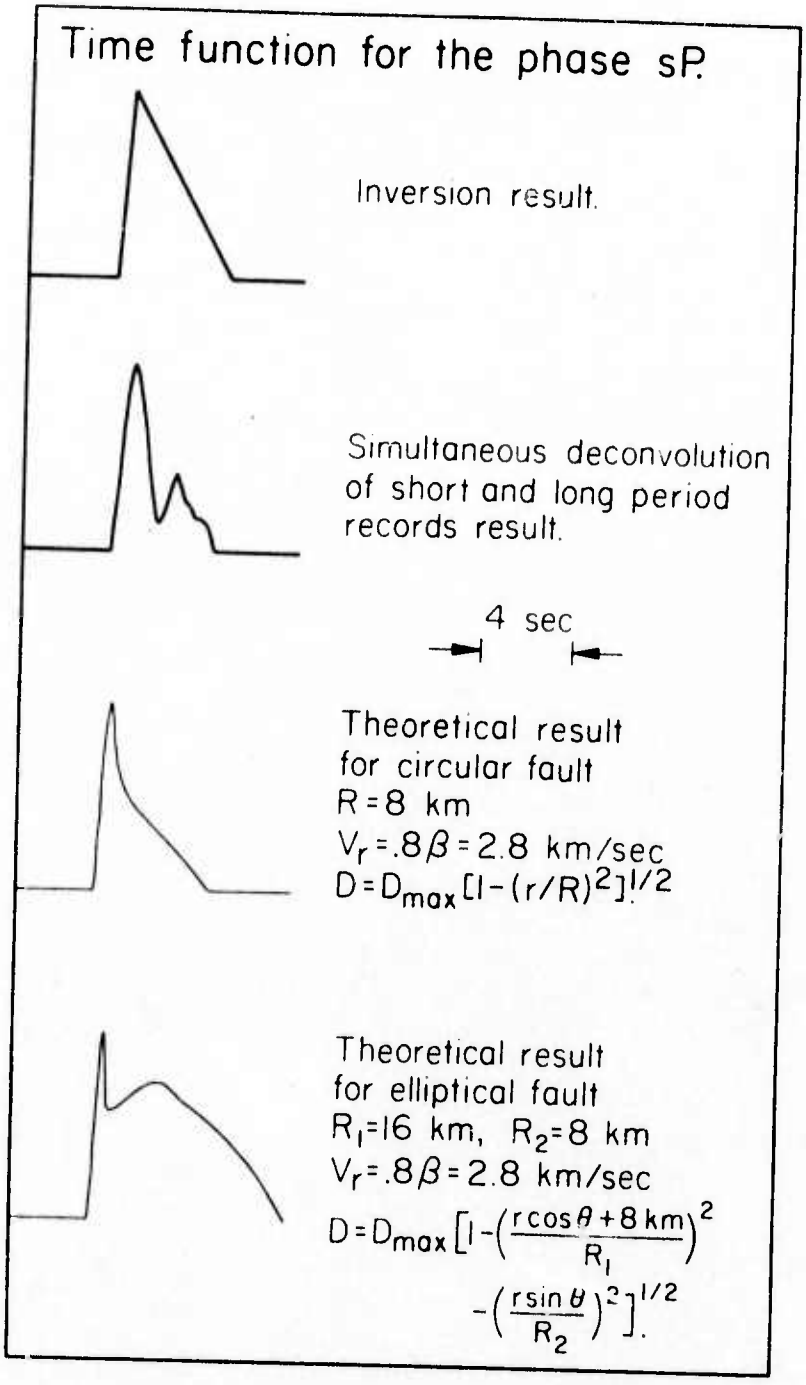

Figure 8. sP time functions for the station WES obtained from inversion and simultaneous short period-long period deconvolution as opposed to theoretical results for a circular fault large enough to extend over segment BC in Figure 1 and on eliptical fault large enough to cover BD. D_{max} is the maximum displacement, and r and θ are cylindrical coordinates on the fault surface. The average time history for the theoretical models is a step function.

The more southern segment showed a much smaller initial offset, extensive postseismic creep, and a higher level of aftershocks. We infer that the southern segment initially absorbed most of the stress load induced by the brittle failure of the north segment but then released it slowly. Some failure must have occurred sometime in the first few hours to account for the initial surface offset observations, but the creep movement extended over a period of months. It seems as though the southern portion of the Borrego event was very similar to the nearby Brawley swarm event

studied by Johnson and Hadley (1976).

The complete synthetic seismograms predicted by the finite source model are the bottom traces in Figure 5. They appear to fit just as well as the ones computed from the point source model. The predicted azimuthal dependence of pulse duration is very slight which explains why this effect was so difficult to observe in the data.

Assuming that the first shock had a moment of 11.2×10^{25} dyne-cm and a radius of about 8 km, and if μ was approximately 3.4×10^{11} $\frac{gm}{cm\ sec^2}$ then the average displacement must have been

$$D_{av} = \frac{M_o}{\mu \pi R^2} = 164cm$$

This value is four times as large as the observed surface offsets implying that the displacements decreased as the rupture propagated upward. Since for the theoretical model considered here displacement varies along the fault as $D = D_{Max}\sqrt{1 - (\frac{r}{R})^2}$, the largest displacement was

$$D_{Max} = \frac{3}{2} D_{av} = 246\ cm$$

Keilis-Borok (1959) has formulated an expression for the stress drop from a dislocation of this type.

Modeling the local strong-motions

Unfortunately, not many broad-band observations are available for the Borrego event because of remote locations. However, an excellent long period response was obtained at El Centro, Δ = 60 km. The SH motion is presented in Figure 9 where the instrument has been removed. Several models have been constructed to fit the first 40 secs of motion. The modeling was done in the time domain using the response computed for point double-couple shear dislocations embedded in a layered half-space as discussed earlier.

It was found that the modeling process is nonunique in that many different models adequately fit the SH broad motion. A 2.9 km thick layer with the velocity of 1.5 km/sec gives a good overall fit to the Love wave portion of the record for a variety of sources at depths ranging from 4 to 10 km. The beginning 10 seconds of record is considerably more sensitive to the source datails than the later portion of the record as found in the Bear Valley study. A simple model compatible with the far-field inversion is displayed in Figure 9 where the high rise time is most evident.

CONCLUSIONS

The purpose of this study was twofold. The first was to identify and characterize all of the different elements which control the shape of the body waves from a shallow earthquake. The second was to isolate an arrival which was not strongly contaminated by other arrivals and to model this single arrival with a finite dislocation source. In pursuing the first of these, we found that reflections from the free surface play a dominant role in shaping the pulse, but also that arrivals from the first large aftershocks could be observed in the waveform. This result is not too remarkable since there is no reason to expect a long delay between the termination of the main shock and the initiation

of the aftershock sequence. In pursuing the second goal, we decided to construct a model for the sP phase from the main shock. A smooth dislocation proved to be adequate to model the pulse just as in the case of most deep earthquakes.

The fault parameters of the Borrego Mountain event were previously determined using the spectral characteristics technique by Hanks and Wyss (1972), and by Wyss and Hanks (1972a). They analyzed the P and S data separately which gave two different values for each parameter. Their moment values of M_o (P) = 10 x 10^{25} dyne-cm and M_o(S) = 6.6 x 10^{25} dyne-cm compare favorably with the value from this study of 11.2 x 10^{25} dyne-cm. However, this agreement is probably fortuitous, since the moments they determined were based on the long period level Ω_o of the amplitude spectrum of the entire P or S waveforms. This means that they interpreted the sum $\Omega_o(P) + \Omega_o(pP) + \Omega_o(sP)$ as though it were only $\Omega_o(P)$ and the sum $\Omega o(S) + \Omega_o(sS) + \Omega_o(pS)$ as though it were only $\Omega_o(S)$. Their values for the fault radius, R(P) = 14 km and R(s) = 23 km, are significantly larger than the R = 8 km result of this study. Therefore, they computed a stress drop $\Delta\sigma$ of only 6 bars as compared to the $\Delta\sigma$ = 96 bars result obtained here. It is encouraging that when the free surface is properly accounted for it is not necessary to use different source parameters for S and P.

The relatively small value of R = 8 km was chosen to give an appropriate fit to the shape and duration of the observed sP pulse. As we have discussed, an 8 km fault radius does not conflict with the postseismic observations, if the CD segment of the fault is assummed to be a creep or swarm event. If this analysis is correct,

it means that it is necessary to be cautious about inferring fault dimensions from rupture lengths or aftershock zones.

Finally, we have demonstrated the adequacy of a shallow double couple point source model in predicting wave shapes. The only breakdowns occur when observations are made near nodes. One of the mechanisms of breakdown is apparently instability in the polarization of the S motion induced by lateral structure. Since sP sometimes dominates the P waveform, this can cause anomalies in the P waves as well as the S waves.

Table 1

Station Location and Amplitude Data

STN	Azimuth from North	Wave Type	Moment $\times 10^{-25}$ dyne-cm	ϕ	Relative Deviation of M_o from Average
MAT	309°	P	17.2	6°	.53
SEO	315°	P	16.0	0°	.42
COL	338°	P	12.3	23°	.09
KEV	13°	P	12.1	58°	.08
KEV	13°	SH	9.5	58°	- .15
NUR	18°	P	13.6	63°	.21
UME	18°	SH	11.2	63°	.00
AKU	27°	SH	10.5	72°	- .06
ESK	33°	SH	10.4	78°	- .07
LOR	36°	SH	10.2	81°	- .09
MAL	48°	SH	10.3	87°	- .09
WES	62°	P	12.3	73°	.09
WES	62°	SH	9.8	73°	- .13
OGD	64°	P	9.9	71°	- .12
OGD	64°	SH	9.3	71°	- .17
SCP	65°	P	11.1	70°	- .01
SCP	65°	SH	8.3	70°	- .26
NAT	100°	P	11.8	35°	.05
BOG	117°	P	18.4	18°	.64
BHP	117°	P	10.0	18°	- .11

Table 1 (cont.)

Station Location and Amplitude Data

STN	Azimuth from North	Wave Type	Moment x 10^{-25} dyne-cm	ϕ	Relative Deviation of M_o from Average
LPB	129°	P	11.6	6°	.03
LPB	129°	SH	9.0	6°	- .20
ARE	132°	P	15.0	3°	.34
ARE	132°	SH	7.1	3°	- .37
NNA	133°	P	12.9	2°	.15
NNA	133°	SH	6.4	2°	- .43
LPA	136°	SH	9.5	1°	- .16
PEL	142°	SH	8.8	7°	- .22

$\bar{M}_o$ = 11.2
σ = 2.8

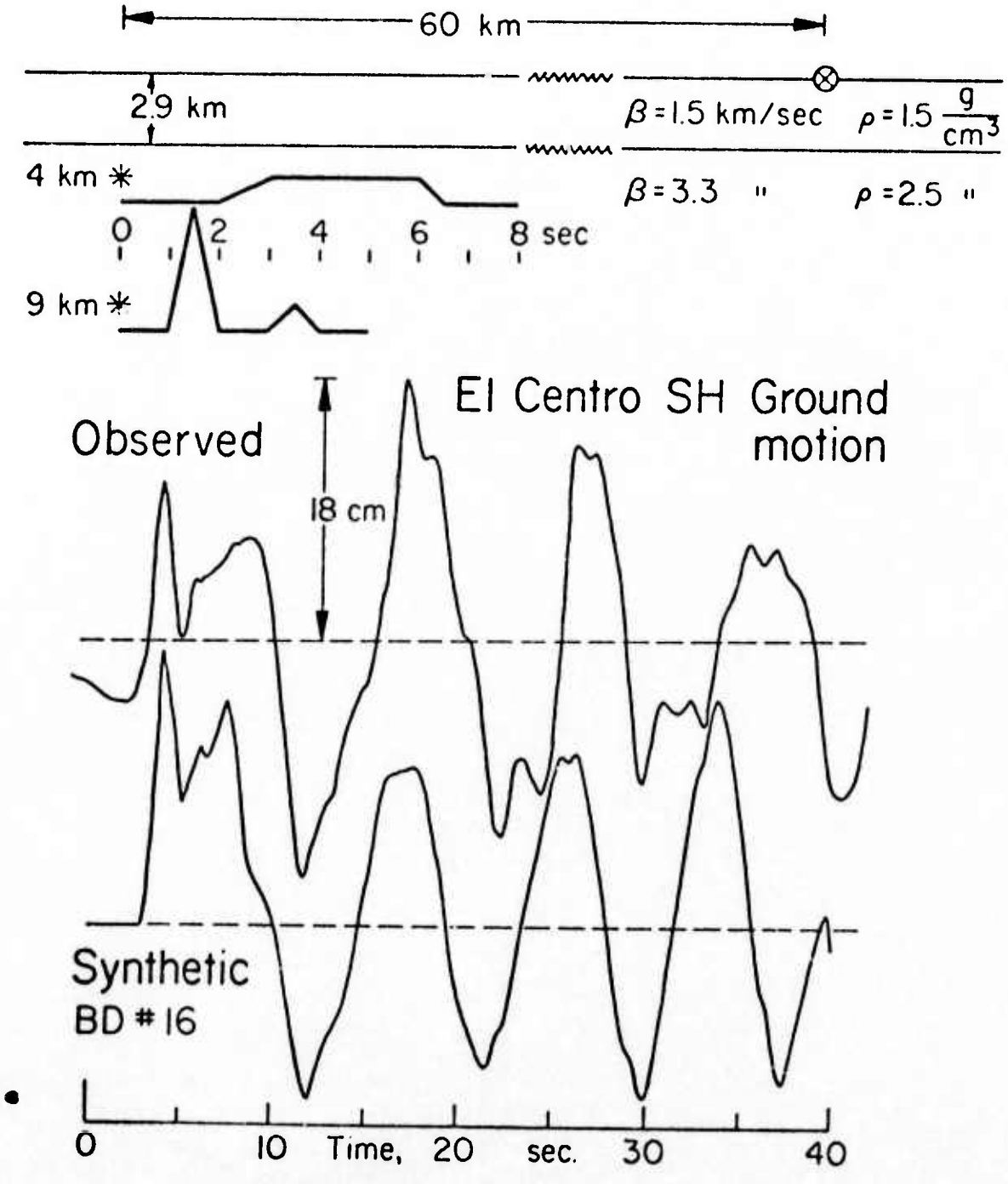

Figure 9. Comparison of synthetic displacement with the observed motion assuming a moment of 1.1×10^{26} dyne-cm.

REFERENCES

Allen, C. R., and J. M. Nordquist (1972) Foreshock, Main Shock and Larger Aftershocks of the Borrego Mountain Earthquake, U. S. Geol. Survey Prof. Paper 787, 16-23.

Allen, C. R., et al (1972). Displacements on the Imperial, Superstition Hills, and San Andreas faults triggered by the Borrego Mountain Earthquake, U. S. Geol. Survey Prof. Paper 787, 87-104.

Boore, D. M. and D. P. Hill (1973). Wave propagation characteristics in the vicinity of the San Andreas fault, Stanford Univ. Pub., Geological Sciences, 13, 214-223.

Brune, J. N. (1970) Tectonic stress and the spectra of seismic shear waves from earthquakes, J. Geophys. Res. 75, 4997-5009.

Burdick, L. and G. Mellman (1976). A determination of the Borrego Mountain earthquake source mechanism using a generalized linear inverse technique.

Burdick, L. J. and D. V. Helmberger(1974). Time Functions Appropriate for Deep Earthquakes, Bull. Seism. Soc. Am., 64, 5, 1419-1428.

Burford, R. O. (1972). Continued slip on the Coyote Creek Fault after the Borrego Mountain Earthquake, U. S. Geol. Survey Prof. Paper 787, 105-111.

Burridge, R.(1969) The numerical solution of certain integral equations with nonintegrable kernals arising in the theory of crack propagation and elastic wave diffraction, Phil. Trans. Roy Soc. (London), Ser. A. 265, 353-381.

Clark, M. M., (1972) Surface ruptures along the Coyote Creek Fault, U. S. Geol. Survey Prof. Paper 787, 55-86.

Fukao, Y.(1971). Seismic body waves from surface faults, J. Phys. Earth, 19, 4, 271-281.

Hamilton, R. M. (1972). Aftershocks of the Borrego Mountain earthquake from April 12 to June 12, 1968, U. S. Geol. Survey Prof. Paper 787, 31-54.

Hanks, T. C. and M. Wyss (1972). The use of body-wave spectra in the determination of seismic-source parameters, Bull. Seism. Soc. Am., 62, 2, 56.-589.

Helmberger, D. V. (1974). Generalized ray theory for shear dislocations, Bull. Seism. Soc. Am., 64, 1, 45-64.

Hudson, J. A. (1969). A quantitative evaluation of seismic signals at teleseismic distances I Radiation from point sources, Geophy. J. R. astr. Soc., 18, 233-249.

Johnson, C. E. and D. M. Hadley (1975). Tectonic implications of the Brawley earthquake swarm, Imperial Valley, California, January 1975, submitted to Bull. Seism. Soc. Am.

Johnson, L. R. (1974). Green's functions for Lanb's problem, Geophys. J. 37, 99-131.

Johnson, L. R. and T. V. McEvilly (1974). Near-Field observations and source parameters of central California earthquakes, Bull. Seism. Soc. Am., 64, 1855-1886.

Kanamori, H. and D. L. Anderson (1975). Theoretical basis of some empirical relations in seismology, Bull. Seism. Soc. Am., 65, 5, 1073-1095.

Keilis-Borok, V. (1959). On estimation of the displacement in an earthquake source and of source dimensions, Ann. Geofis. (Rome) 12, 205-214.

Langston, C. A. and D. V. Helmberger (1975). A procedure for modelling shallow dislocation sources, Geophys. J. R. astr. Soc., 42, 117-130.

Madaraiga, R., Dynamics of an expanding circular fault, submitted to Bull. Seism. Soc. Am.

Mellman, G. and L. J. Burdick (1976). Inversion of body waves to fault models, in preparation.

Mellman, G. and D. V. Helmberger (1974). High-frequency attenuation by a thin high-velocity layer, Bull. Seism. Soc. Am., 64, 1383-1388.

Mikumo, T. (1971). Source processes of deep and intermediate earthquakes as inferred from long period P and S waveforms, J. Phys. Earth 19, 4. 303-320.

Mikumo, T. (1971). Source processes of deep and intermediate depth earthquakes as inferred from long period P and S waveforms I, J. Phys. Earth, 19, 1, 1-19.

Molnar, P., Tucker, B. E., and J. N. Brune (1973). Corner frequencies of P and S waves and models of earthquake sources, Bull. Seism. Soc. Am., 63, 6, 2091-2104.

Molnar, P.and M. Wyss, (1972). Moments, source dimensions and stress drops of shallow focus earthquakes in the Tonga-Kermadec Arc, Phys. Earth Planet Interiors, 6, 263-278.

Savage,J. C.(1966). Radiation from a realistic model of faulting, Bull. Seism. Soc. Am., 56, 2, 577-592.

Sharp, R. V. (1972). Tectonic setting of the Salton Trough, U. S. Geol. Survey Prof. Paper 787, 3-15.

Teng, T. L., and A. Ben-Menahem (1965). Mechanism of deep earthquakes from spectrums of isolated body wave signals, J. Geophys. Res., 70, 20, 5157-5170.

Thatcher, W. and T. C. Hanks (1973). Source parameters of southern California Earthquakes. J. Geophys. Res., 78, 8547-8576.

Wyss, M. and T. C. Hanks (1972). Source parameters of the Borrego Mountain earthquake, U. S.Geol. Survey Prof. Paper 787, 24-30.

Wyss, M. and T. C. Hanks (1972). The source parameters of the San Fernando earthquake inferred from teleseismic body waves, Bull. Seism. Soc. Am., 62, 2.

REFERENCES

Allen, C. R., and J. M. Nordquist (1972) Foreshock, Main Shock and Larger Aftershocks of the Borrego Mountain Earthquake, U. S. Geol. Survey Prof. Paper 787, 16-23.

Allen, C. R., et al (1972). Displacements on the Imperial, Superstition Hills, and San Andreas faults triggered by the Borrego Mountain Earthquake, U. S. Geol. Survey Prof. Paper 787, 87-104.

Boore, D. M. and D. P. Hill (1973). Wave propagation characteristics in the vicinity of the San Andreas fault, Stanford Univ. Pub., Geological Sciences, 13, 214-223.

Brune, J. N. (1970) Tectonic stress and the spectra of seismic shear waves from earthquakes, J. Geophys. Res. 75, 4997-5009.

Burdick, L. and G. Mellman (1976). A determination of the Borrego Mountain earthquake source mechanism using a generalized linear inverse technique.

Burdick, L. J. and D. V. Helmberger(1974). Time Functions Appropriate for Deep Earthquakes, Bull. Seism. Soc. Am., 64, 5, 1419-1428.

Burford, R. O. (1972). Continued slip on the Coyote Creek Fault after the Borrego Mountain Earthquake, U. S. Geol. Survey Prof. Paper 787, 105-111.

Burridge, R.(1969) The numerical solution of certain integral equations with nonintegrable kernals arising in the theory of crack propagation and elastic wave diffraction, Phil. Trans. Roy Soc. (London), Ser. A. 265, 353-381.

Clark, M. M., (1972) Surface ruptures along the Coyote Creek Fault, U. S. Geol. Survey Prof. Paper 787, 55-86.

Fukao, Y.(1971). Seismic body waves from surface faults, J. Phys. Earth, 19, 4, 271-281.

Hamilton, R. M. (1972). Aftershocks of the Borrego Mountain earthquake from April 12 to June 12, 1968, U. S. Geol. Survey Prof. Paper 787, 31-54.

Hanks, T. C. and M. Wyss (1972). The use of body-wave spectra in the determination of seismic-source parameters, Bull. Seism. Soc. Am., 62, 2, 56.-589.

Helmberger, D. V. (1974). Generalized ray theory for shear dislocations, Bull. Seism. Soc. Am., 64, 1, 45-64.

Hudson, J. A. (1969). A quantitative evaluation of seismic signals at teleseismic distances I Radiation from point sources, Geophy. J. R. astr. Soc., 18, 233-249.

Johnson, C. E. and D. M. Hadley (1975). Tectonic implications of the Brawley earthquake swarm, Imperial Valley, California, January 1975, submitted to Bull. Seism. Soc. Am.

Johnson, L. R. (1974). Green's functions for Lanb's problem, Geophys. J. 37, 99-131.

Johnson, L. R. and T. V. McEvilly (1974). Near-Field observations and source parameters of central California earthquakes, Bull. Seism. Soc. Am., 64, 1855-1886.

Kanamori, H. and D. L. Anderson (1975). Theoretical basis of some empirical relations in seismology, Bull. Seism. Soc. Am., 65, 5, 1073-1095.

Keilis-Borok, V. (1959). On estimation of the displacement in an earthquake source and of source dimensions, Ann. Geofis. (Rome) 12, 205-214.

Langston, C. A. and D. V. Helmberger (1975). A procedure for modelling shallow dislocation sources, Geophys. J. R. astr. Soc., 42, 117-130.

Madaraiga, R., Dynamics of an expanding circular fault, submitted to Bull. Seism. Soc. Am.

Mellman, G. and L. J. Burdick (1976). Inversion of body waves to fault models, in preparation.

Mellman, G. and D. V. Helmberger (1974). High-frequency attenuation by a thin high-velocity layer, Bull. Seism. Soc. Am., 64, 1383-1388.

Mikumo, T. (1971). Source processes of deep and intermediate earthquakes as inferred from long period P and S waveforms, J. Phys. Earth 19, 4. 303-320.

Mikumo, T. (1971). Source processes of deep and intermediate depth earthquakes as inferred from long period P and S waveforms I, J. Phys. Earth, 19, 1, 1-19.

Molnar, P., Tucker, B. E., and J. N. Brune (1973). Corner frequencies of P and S waves and models of earthquake sources, Bull. Seism. Soc. Am.. 63, 6, 2091-2104.

Molnar, P.and M. Wyss, (1972). Moments, source dimensions and stress drops of shallow focus earthquakes in the Tonga-Kermadec Arc, Phys. Earth Planet Interiors, 6, 263-278.

Savage,J. C.(1966). Radiation from a realistic model of faulting, Bull. Seism. Soc. Am., 56, 2, 577-592.

Sharp, R. V. (1972). Tectonic setting of the Salton Trough, U. S. Geol. Survey Prof. Paper 787, 3-15.

Teng, T. L., and A. Ben-Menahem (1965). Mechanism of deep earthquakes from spectrums of isolated body wave signals, J. Geophys. Res., 70, 20, 5157-5170.

Thatcher, W. and T. C. Hanks (1973). Source parameters of southern California Earthquakes. J. Geophys. Res., 78, 8547-8576.

Wyss, M. and T. C. Hanks (1972). Source parameters of the Borrego Mountain earthquake, U. S.Geol. Survey Prof. Paper 787, 24-30.

Wyss, M. and T. C. Hanks (1972). The source parameters of the San Fernando earthquake inferred from teleseismic body waves, Bull. Seism. Soc. Am., 62, 2.

UNCLASSIFIED
SECURITY CLASSIFICATION OF THIS PAGE (When Data Entered)

REPORT DOCUMENTATION PAGE

READ INSTRUCTIONS BEFORE COMPLETING FORM

1. REPORT NUMBER (19) AFOSR-TR-76-0337	2. GOVT ACCESSION NO.
3. RECIPIENT'S CATALOG NUMBER	
4. TITLE (and Subtitle) (6) Near Field Small Earthquake Long Period Array,	5. TYPE OF REPORT & PERIOD COVERED (9) Scientific Final Rept. 1 Jun 72 - 30 Nov 75,
6. PERFORMING ORG. REPORT NUMBER	
7. AUTHOR(s) (10) Charles B. Archambeau, Donald V. Helmberger (11) 1976	8. CONTRACT OR GRANT NUMBER(s) (15) F44620-72-C-0083, ARPA Order-2134
9. PERFORMING ORGANIZATION NAME AND ADDRESS California Institute of Technology, Seismological Laboratory, Pasadena, California 91109 (12) 71p.	10. PROGRAM ELEMENT, PROJECT, TASK AREA & WORK UNIT NUMBERS AO 2134 2F10
11. CONTROLLING OFFICE NAME AND ADDRESS ARPA/NMR, 1400 Wilson Blvd., Arlington, VA 22209	12. REPORT DATE 76
	13. NUMBER OF PAGES 70
14. MONITORING AGENCY NAME & ADDRESS (if different from Controlling Office) AFOSR/NP, Bolling AFB, Wash DC 20332	15. SECURITY CLASS. (of this report) Unclassified
	15a. DECLASSIFICATION/DOWNGRADING SCHEDULE

16. DISTRIBUTION STATEMENT (of this Report)

Approved for public release;
distribution unlimited.

17. DISTRIBUTION STATEMENT (of the abstract entered in Block 20, if different from Report)

18. SUPPLEMENTARY NOTES

TECH, OTHER

19. KEY WORDS (Continue on reverse side if necessary and identify by block number)

20. ABSTRACT (Continue on reverse side if necessary and identify by block number)

This final report describes the accomplishments achieved during the last year of our efforts towards a better understanding of the seismic radiation from earthquakes. Applying the techniques discussed in earlier reports on calculating the synthetic response generated by shear dislocation sources in a layered media we have endeavored to separate source effects from those due to propagation in the earth. The main objective here is an accurate scaling law of duration versus moment to be used in discrimination studies. The observations used in this report are of two types, those that are large enough to be

DD FORM 1 JAN 73 1473 EDITION OF 1 NOV 65 IS OBSOLETE

320 050

SECURITY CLASSIFICATION OF THIS PAGE (When Data Entered)

studied teleseismically where one must separate the phases P, pP and sP etc., and those that are too small to be observed at large distances and must be studied locally. Thus our efforts have been divided into two sections, to model local broadband observations of moderate size earthquakes, and secondly, to apply our recently developed generalized inversion theory to the problem of obtaining source determinations based on teleseismic long and short period body waves. In collaboration with Lane Johnson we investigated some of his broadband observations of central California earthquakes as recorded on opposite sides of the San Andreas fault zone. The earthquake mechanisms were of the strike-slip type occurring along the fault at epicentral distances less than 30 km. The seismograms obtained at the two sites are distinctly dissimilar in waveshape and amplitude even though they are at roughly the same azimuth. We found that these effects can be explained by a two layer upper-crustal model appropriate for each site. The results determined by matching the observations synthetically indicate that the durations for these events with M_L = 3.5 to 5 are about.3 to .6 seconds respectively and that accurate estimates of such parameters can only be accomplished after a detailed appreciation of receiver structure. For the large events, magnitudes greater than 6, we adapted a generalized linear inverse technique for determining the source parameters from body wave data at teleseismic ranges, = 30 to 90 degrees. The technique has been applied successfully to several events but we will restrict ourselves in this report to Borrego Mountain earthquake of April 9, 1968. Synthetic seismograms computed from the resulting model match in close detail the first 25 seconds of long period seismograms from a wide range of azimuths. The main shock source time function has been determined by a new simultaneous short period-long period deconvolution technique as well as by the inversion technique. The duration and shape of this time function indicate that most of the body wave energy was radiated from a surface with effective radius of only 8 km. This is much smaller than the total surface rupture length of the length of the aftershock zone. Along with the moment determination of M_o = 11.2 x 10^{25} dyne-cm, this radius implies a high stress drop of about 96 bars. A plot of stress drop versus duration for events determined by fitting waveforms in the time-domain suggests that larger events may have higher stress drops than smaller events at least for the California examined in this report.